



Di-aryl guanidinium derivatives: Towards improved α_2 -Adrenergic affinity and antagonist activity



Michela McMullan^a, Brendan Kelly^{b,c}, Helene B. Mihigo^a, Aaron P. Keogh^a,
Fernando Rodriguez^a, Iria Brocos-Mosquera^{d,e}, Aintzane García-Bea^d,
Patricia Miranda-Azpiazu^d, Luis F. Callado^{d,e}, Isabel Rozas^{a,*}

^a School of Chemistry, Trinity Biomedical Sciences Institute, Trinity College Dublin, 152-160, Pearse Street, Dublin 2, Ireland

^b Department of Computer Science, Molecular and Cellular Physiology, Institute for Computational and Mathematical Engineering, Stanford University, Stanford, CA, 94305, USA

^c Department of Structural Biology, Institute for Computational and Mathematical Engineering, Stanford University, Stanford, CA, 94305, USA

^d Department of Pharmacology, University of the Basque Country, UPV/EHU, Leioa, Bizkaia, Spain

^e Centro de Investigación Biomédica en Red de Salud Mental (CIBERSAM), Spain

ARTICLE INFO

Article history:

Received 3 July 2020

Received in revised form

18 September 2020

Accepted 13 October 2020

Available online 24 October 2020

Keywords:

Di-phenyl methane

Di-pyridin-2-yl methane

Benzylpyridin-2-yl

Guanidine

2-aminoimidazoline

Depression

α_2 -adrenoceptor ligands

α_2 -adrenoceptor antagonists

Human brain tissue *in vitro* experiments

Molecular modelling

ABSTRACT

Compounds with excellent receptor engagement displaying α_2 -AR antagonist activity are useful not only for therapeutic purposes (e.g. antidepressants), but also to help in the crystallization of this particular GPCR. Therefore, based on our broad experience in the topic, we have prepared eighteen di-aryl (phenyl and/or pyridin-2-yl) mono- or di-substituted guanidines and 2-aminoimidazolines. The *in vitro* α_2 -AR binding affinity experiments in human brain tissue showed the advantage of a 2-aminoimidazolium cation, a di-arylmethylene core, a conformationally locked pyridin-2-yl-guanidine and a di-substituted guanidinium to achieve good α_2 -AR engagement. After different *in vitro* [³⁵S]GTP γ S binding experiments in human prefrontal cortex tissue, it was possible to identify that compounds **7a**, **7b** and **7c** were α_2 -AR partial agonist, whereas **8h** was a potent α_2 -AR antagonist. Docking and MD studies with a model of α_{2A} -AR and two crystal structures suggest that antagonism is achieved by compounds carrying a di-substituted guanidine which substituent occupy a pocket adjacent to TM5 without engaging S200^{5,42} or S204^{5,46}, and a mono-substituted cationic group, which favorably interacts with E94^{2,65}.

© 2021 The Authors. Published by Elsevier Masson SAS. This is an open access article under the CC BY license (<http://creativecommons.org/licenses/by/4.0/>).

1. Introduction

Although in recent years there has been a huge advancement in understanding neural regions and circuits implicated in stress responses of affective disorders such as depression [1–3], there is still limited novel treatments to show for it. Pharmacological manipulation of monoamine transmission remains the most successful

therapeutic approach to date [4], and it is now accepted that this alteration in chemical concentration indirectly induces the gradual strengthening of synapses (neuroplasticity) and synthesis of new neurons (neurogenesis) over the course of treatment to elicit the behavioural antidepressant response [5].

Noradrenergic transmission plays a central role in the mediation of stress where alterations in its signalling as well as changes in physical features of its plasticity are heavily implicated in stress-related disorders [6]. Dysfunction of noradrenergic transmission in these disorders has been hypothesised to be directly linked to the α_2 -noradrenergic receptor (α_2 -AR), as post-mortem biochemical assays as well as live patient models have illustrated an up-regulation or increase in receptor density of the high-affinity state of the α_2 -AR in depression [7,8]. This is further supported by the effects of normal antidepressant treatments which have shown

List of abbreviations: α_2 -ARs, α_2 -adrenoceptors; nBuLi, n-butyl lithium; Boc, tert-butoxycarbonyl; Fmoc, Fluorenylmethyloxycarbonyl; PFC, prefrontal cortex; [³H]RX821002, 2-methoxyidazoxan; K_i, inhibition constant; [³⁵S]GTP γ S, radioligand guanosine 5'-O-[gamma-thio]triphosphate; GPCR, G-protein coupled receptor; EC₅₀, Half maximal effective concentration; E_{max}, maximum [³⁵S]GTP γ S binding stimulation over basal; IMHB, intramolecular hydrogen bond.

* Corresponding author.

E-mail address: rozasi@tcd.ie (I. Rozas).

to desensitize or down-regulate the increase in α_2 -AR density [9]. Clinical α_2 -AR antagonists have shown to have faster behavioural antidepressant responses than conventional antidepressants alone, which are thought to be due to a combination of their effects on noradrenaline transmission, as well as influencing key responses involved in neuroplasticity and neurogenesis.

Our group has been interested in the development of aryl guanidines as antagonists of the α_2 -ARs for more than 15 years [10–15]. Thus, in a previous study the di-phenylmethane bis-2-aminoimidazolium compound **1** (Fig. 1) was identified as a 'hit' [11], because, even though it was an agonist, it showed excellent α_2 -AR binding affinity ($K_i = 1.58$ nM). From these studies, shorter monomeric analogues were prepared exhibiting reasonable affinities (<300 nM K_i values), yet discrepancies between agonist and antagonist activity were seen amongst very structurally similar derivatives (**2** and **3**, Fig. 1) [11–14].

Activity at the receptor is of paramount importance; therefore, our group developed a 3D pharmacophore incorporating a wide range of α_2 -AR antagonists, to underline the structural elements needed for antagonistic activity [13]. This study indicated the requirements of R^2 substitution at the guanidinium moiety (**4**, Fig. 1) resulting in ligands with exclusive antagonist activity. However, it must be noted that this modification had a detrimental effect on the α_2 -AR affinity. Later, we reported a series of pyridinyl guanidine and 2-aminoimidazoline derivatives (**5**, Fig. 1) as conformationally controlled systems that showed markedly improved α_2 -AR affinity and, again, consistent antagonist activity [14].

Now, we present the synthesis of a series of di-arylmethane guanidines and 2-aminoimidazolines emanating from the promising pharmacological profiles of initial derivatives as well as the pharmacological evaluation of their *in vitro* α_2 -AR binding affinity and activity in human PFC brain tissue. The primary aim of this work is to obtain compounds with binding affinities in the range of compound **1** (excellent receptor engagement), while displaying solely antagonist activity at the α_2 -AR (selective blockade).

2. Results and discussion

To date no ligand of our in-house library has surpassed the α_2 -AR binding affinity of our initial 'hit' compound **1** ($K_i = 1.58$ nM) and considering that our objective is to prepare high affinity (low

nM K_i values) antagonists of the α_2 -AR, we focused our attention around the di-aryl core of **1**. In a ligand-based drug design strategy, we incorporated key elements from our previously developed pharmacophore and functional modifications that favor α_2 -AR antagonist activity such as the di-substitution of both guanidine functionalities (compounds **6a-c**, Fig. 2). Additionally, since we previously established that the 2-aminoimidazoline derivatives exhibit strong α_2 -AR binding, it was decided to combine these two structural features to create asymmetric di-substituted di-aryl guanidine/2-aminoimidazoline analogues (compounds **7a-f**, Fig. 2). Also, in order to probe if flexibility between the aryl rings is important, compounds with a methylene linker as in 'hit' **1** (**7a-c**, Fig. 2) and an ethylene linker (**7d-f**, Fig. 2) were investigated, since good α_2 -AR antagonist activity has been obtained for previously prepared ethylene linked di-phenyl molecules [11].

Lastly, considering the encouraging results obtained in our previous pyridine *mono*-cation series (compounds **5**, Fig. 1), this bioisosteric modification was also incorporated into the core di-aromatic framework, combining the guanidine and 2-aminoimidazoline moieties on either side of di-pyridin-2-yl or phenyl/pyridine-2-yl systems (compounds **8a-i**, Fig. 2).

2.1. Synthesis

Our usual synthetic pathway towards the guanidine-like derivatives involves the mercury(II) chloride mediated guanidylation of the corresponding di-aryl amines. In the case of compounds **6a-c**, the corresponding starting di-aniline is commercially available; however, the proposed phenyl pyridinyl (**8d-i**) and di-pyridinyl (**8a-c**) guanidine-like derivatives required the initial preparation of the appropriate diamines (**9** and **10**, respectively) from available 2-aminopyridine starting materials (Scheme 1).

The synthesis of phenylpyridinyl diamine **9** involved the preparation of the di-benzyl protected 2-amino-5-bromopyridine (**11**), which was then subjected to lithium halogen exchange using *n*BuLi, and subsequently reacted with 4-nitrobenzaldehyde to give intermediate **12**. Dual reduction of the alcohol and nitro groups under hydrogenation conditions afforded intermediate **13**. It must be noted that the benzyl groups of these 2-amino pyridine analogues were found to be inert to cleavage under hydrogenation conditions up to 12 atm. De-benzylation was next achieved using concentrated

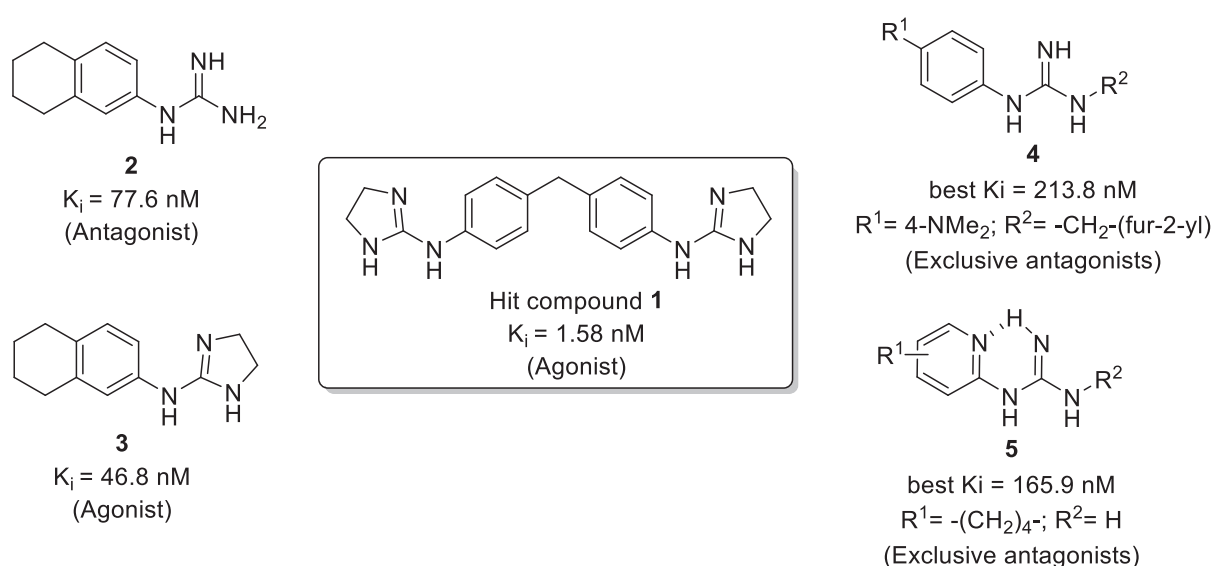


Fig. 1. Structures of some α_2 -AR ligands previously described in our group highlighting structural features necessary for antagonist activity.

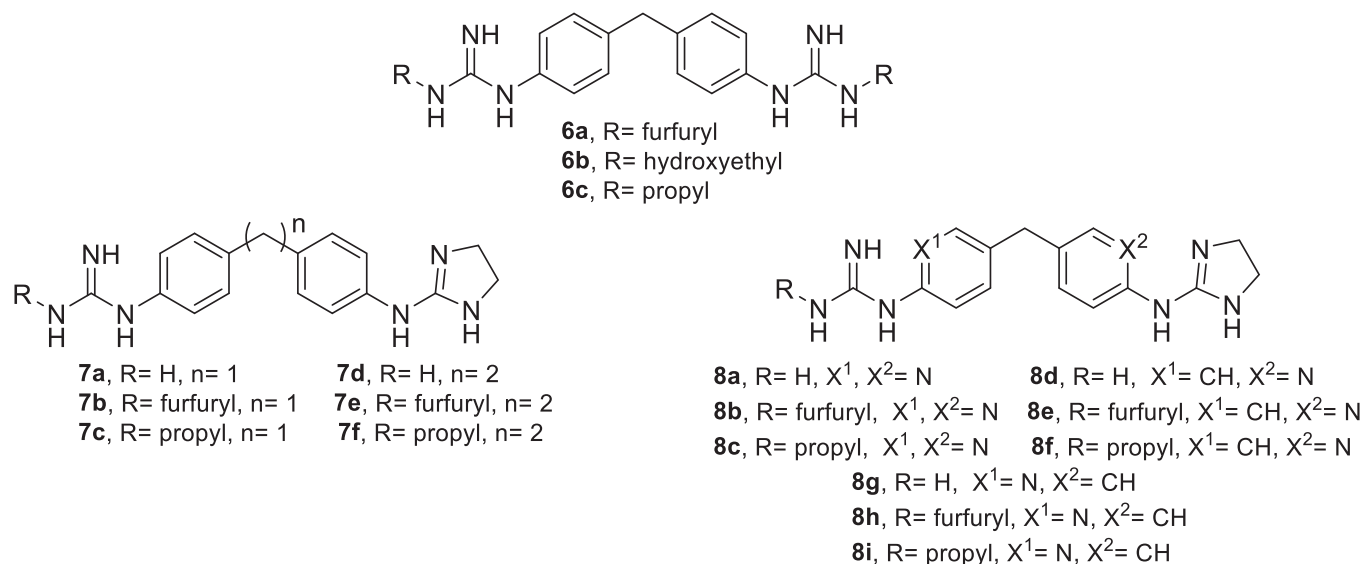
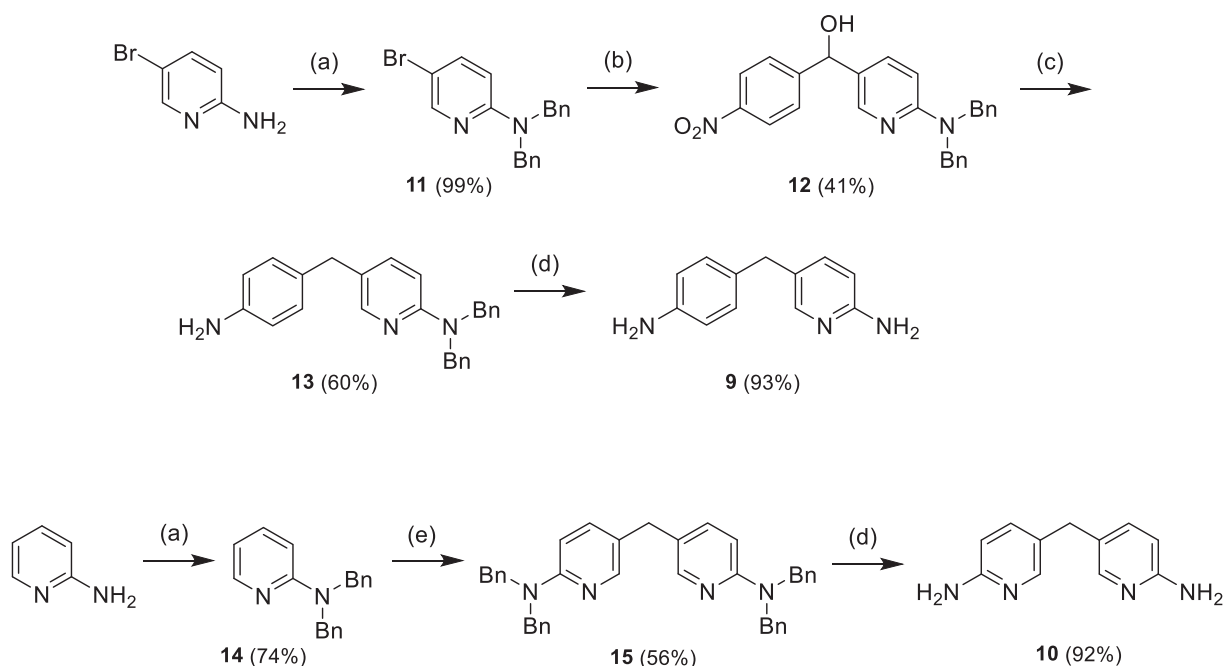


Fig. 2. Structures of the di-aryl methane bis-guanidine (compounds **6a-c**) and guanidine/2-aminoimidazoline (compounds **7a-f** and **8a-i**) families synthesised and investigated as potential α_2 -AR ligands.



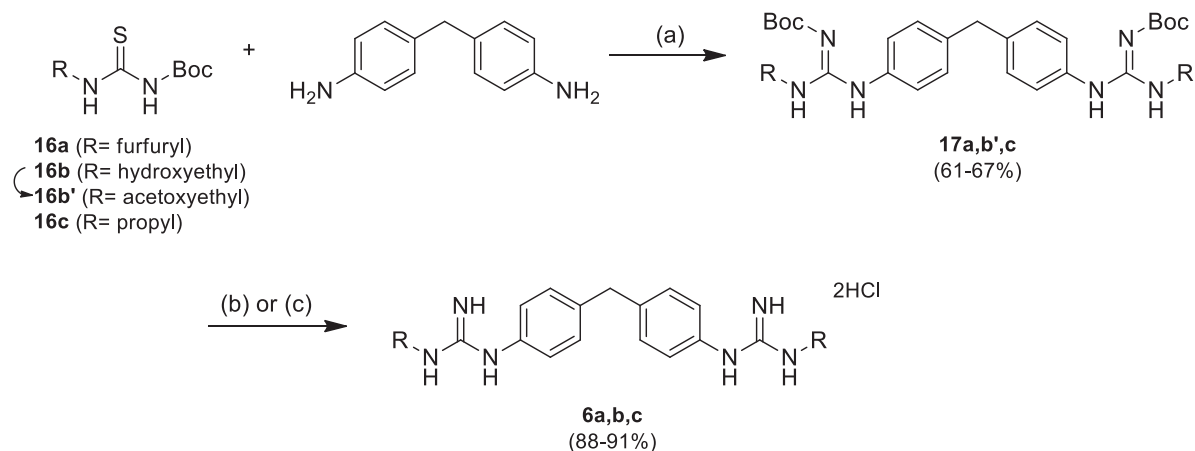
Scheme 1. Synthesis of di-aryl bis-amino precursors **9** and **10**.

sulfuric acid affording diamine **9**. Synthesis of di-pyridinyl diamine **10** involved a modification of literature procedures [16]. The adapted pathway involved the di-benylation of 2-amino pyridine affording **14**, followed by electrophilic aromatic substitution with formaldehyde (37% solution in water) employing acetic acid as an electrophilic assistant. De-benylation was subsequently achieved by stirring **15** in concentrated sulfuric acid for 24 h affording **10** in good yield.

Next, reaction of these starting di-aryl amines with the appropriate mono/di-Boc protected thioureas (**16a,b',c,d**, Schemes 2 and 3; preparation described in ESI) yielded the corresponding Boc-protected bis-guanidylated (**17a,b',c**, Scheme 2) or mono-guanidylated (**18a-l**, Scheme 3) products, depending on the equivalents of amine used.

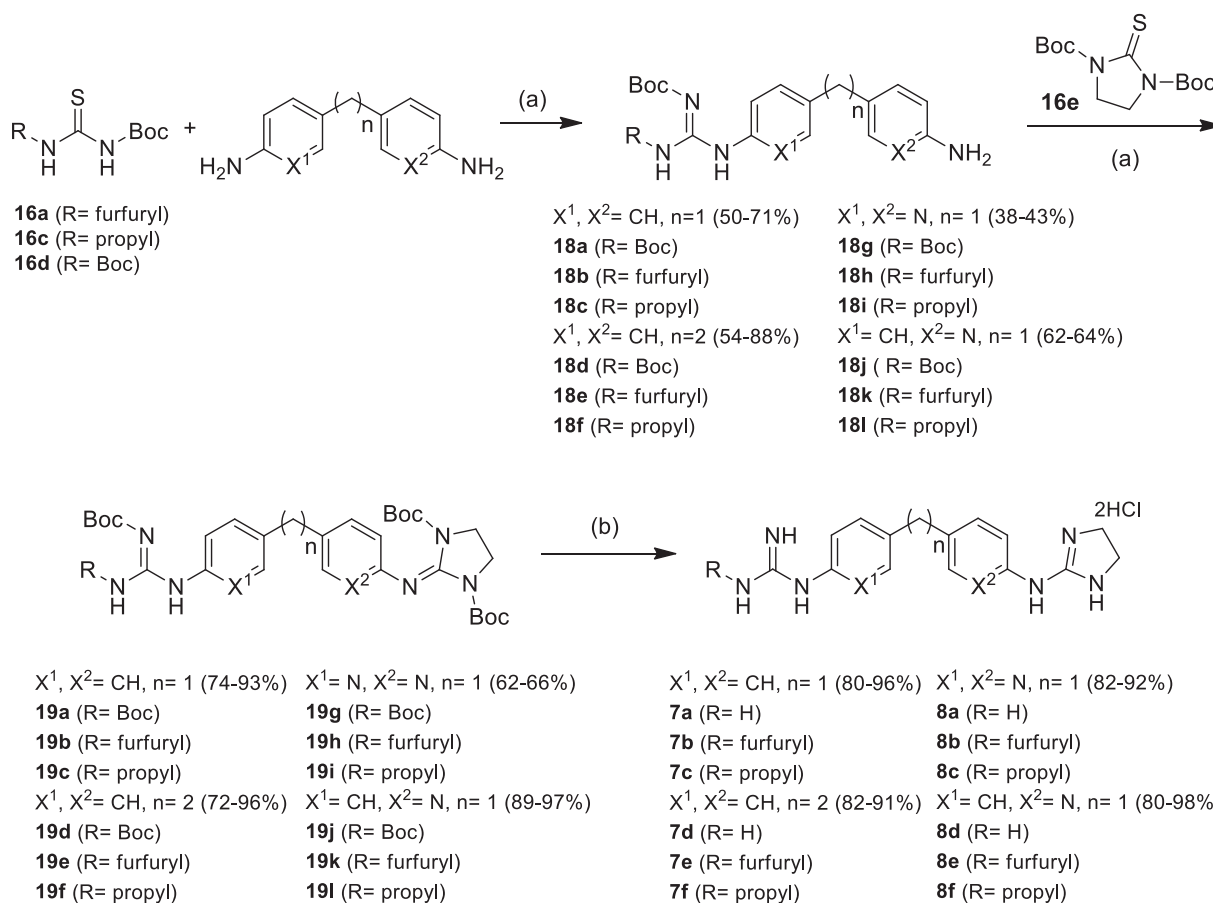
The mono-guanidylated di-aryl amines (**18a-l**) were then subjected to a second coupling reaction with *N,N'*-di(*tert*-butoxycarbonyl)imidazolidine-2-thione in the presence of mercury (II) chloride (Scheme 3) to give the final Boc-protected imino-2-imidazolidine intermediates (**19a-l**). The Boc-protected derivatives were subsequently deprotected using either a 4 M solution of HCl/dioxane or 1.25 M HCl/MeOH to yield the final guanidinium hydrochloride salts (**6a-c**, **7a-f**, and **8a-f**) in excellent yield (Schemes 2 and 3).

Preparation of the pyridin-2-ylguanidine di-aryl derivatives (**8g-i**) is shown in Scheme 4. Ideally, the bis-Boc protected 2-iminoimidazolidine system would be first introduced to the phenyl ring of compound **9** prior to the guanidine, as the aniline



(a) HgCl₂; NEt₃; CH₂Cl₂; r.t. (b) 4M HCl/Dioxane; ⁱPrOH/CH₂Cl₂; r.t.; (c) 1.25M HCl/MeOH; r.t.

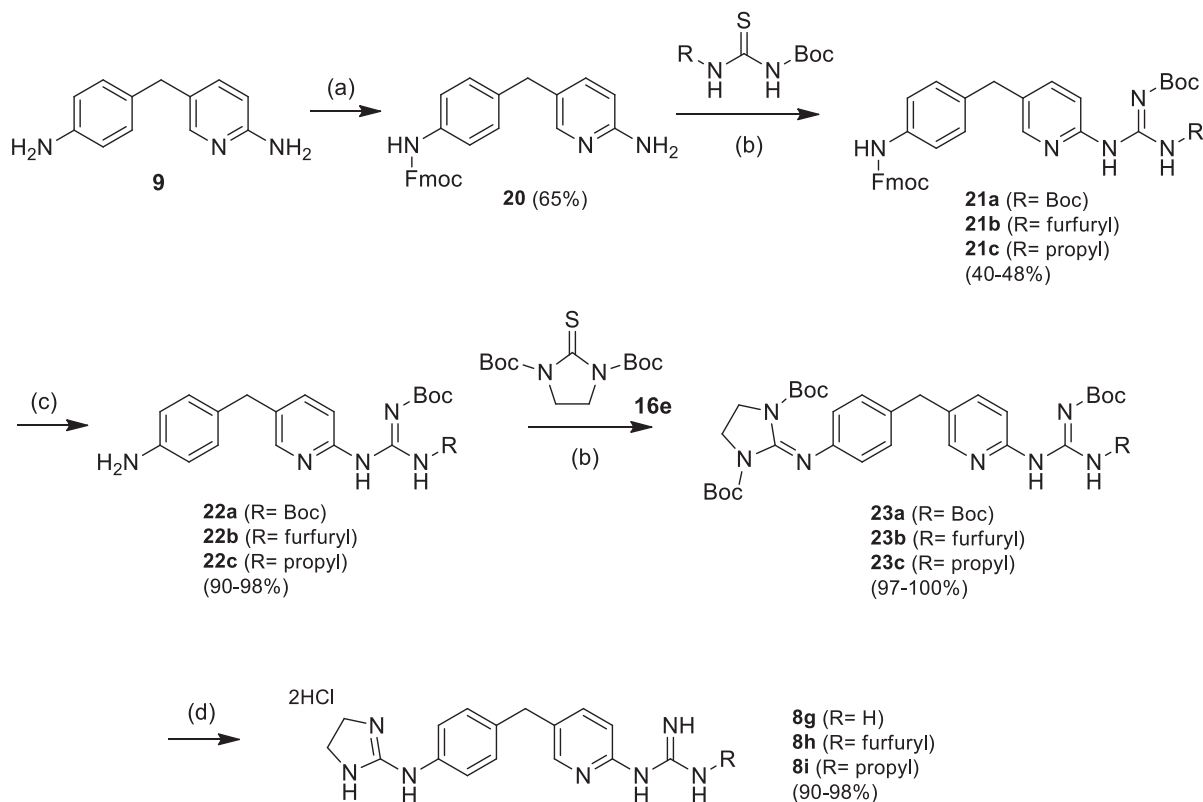
Scheme 2. Synthesis of di-substituted bis-guanidinium di-phenyl derivatives **6a,b,c**.



Scheme 3. Synthesis of guanidinium/2-aminoimidazolium di-aryl derivatives **7a-f** and **8a-f**.

amino group is far more nucleophilic than the 2-aminopyridine amine. Unfortunately, in this situation the 2-iminoimidazolidine moiety is not stable under the guanidylation conditions and leads to degradation products under mercury(II) chloride and other reagents that promote desulphurisation.

Hence, for analogues **8g-i**, di-aryl amine **9** was initially Fmoc protected affording amine **20**, which was then subjected to standard guanidylation conditions with thioureas **16a,c-d** to yield intermediates **21a-c** (Scheme 4). After Fmoc deprotection using excess diethylamine, derivatives **22a-c** were guanidylated with



(a) Pyridine; Fmoc-Cl; THF; r.t. (b) HgCl₂; NEt₃; CH₂Cl₂; r.t. (c) NHEt₂; MeCN; r.t. (d) 4M HCl/Dioxane; ⁱPrOH/CH₂Cl₂; r.t.

Scheme 4. Synthesis of guanidinium/2-aminoimidazolium di-aryl derivatives **8g-i**

N,N'-di(*tert*-butoxycarbonyl)imidazolidine-2-thione affording intermediates **23a-c**, which were subsequently Boc-deprotected to the guanidinium salts (**8g-i**) using hydrochloric acid dioxane solutions (Scheme 4).

2.2. Pharmacology

2.2.1. Binding affinity for the α_2 -AR

The affinity toward α_2 -AR, in general, was measured *in vitro* using human brain PFC tissue by competition assays against the selective radioligand [³H]RX821002 (2-methoxyidazoxan), which has a known high affinity for the α_2 -AR ($K_d = 0.89$ nM) [17]. The PFC region contains α_2 -ARs of different subtypes; however, the α_{2A} -subtype is predominant (90–95%) with a reduced presence of the α_{2C} -subtype (5–10%). Even though there are cell-based assays that allow to assess α_2 -AR subtype selectivity, some previous works (e.g. reference [18]) have shown that selectivity and efficacy demonstrated by different compounds in cell models do not always correspond to those in native tissue itself. Thus, in our study we have focused in the affinity of our compounds for the α_2 -ARs, in general, more than in their selectivity for a specific subtype. In the mentioned competition assay, the prepared membranes containing the receptor proteins were incubated with the radioligand, at a constant concentration of 2 nM. The results obtained (Table 1) are expressed in terms of nM K_i values.

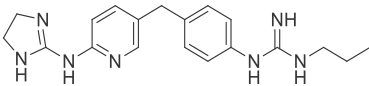
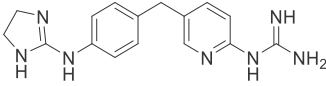
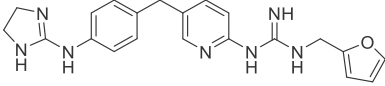
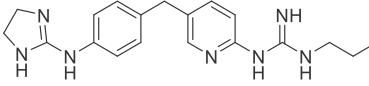
Evaluation of the binding affinities of all di-cationic compounds indicates that, in general, the presence of a 2-aminoimidazoline functional group as one of the cationic components is required to achieve good α_2 -AR engagement ($K_i < 500$ nM), as significantly lower binding affinities were obtained for bis-guanidines **6a-c**. Moreover, the ethylene linked derivatives **7d-f** exhibited poorer affinities compared to the methylene linked analogues **7a-c**; from previous work we have found that alternate linkers such as NH, O, CO or S also result in weaker binding [10], which highlights the advantage of the CH₂ linker for optimal α_2 -AR affinities. In particular, the di-phenyl *N,N'*-bis/mono-substituted guanidine and 2-aminoimidazolidine derivatives **7a-c** gave excellent α_2 -AR binding affinities with the K_i values of **7b-c** on par with that of 'hit' compound **1**. This illustrates that steric extension at the guanidinium moiety can result in higher affinities than the mono-substituted guanidines within the di-cationic series.

In order to analyse the binding results obtained for the family of compounds **8** (Table 1), we should consider first that the potential formation of an IMHB implies a competition for the corresponding cation (guanidinium/2-aminoimidazolium) to interact inter- or intra-molecularly and that could decrease the target engagement. On the contrary, free rotation of the cation indicates that only intermolecular interactions are possible and, hence, a stronger engagement can be achieved. Thus, there are three possible scenarios for the structures of compounds **8**: (i) compounds **8a-c**

Table 1
K_i (nM) values for the α₂-AR shown by all final salts prepared and 'hit' compound 1.

Compound	Structure	K _i (nM) ±SEM
1		1.58 ± 0.12
6a		355 ± 43
6b		2485 ± 372
6c		742 ± 59
7a		12.30 ± 1.11
7b		1.77 ± 0.21
7c		0.82 ± 0.09
7d		175 ± 14
7e		418 ± 50
7f		1745 ± 262
8a		138 ± 11
8b		263 ± 29
8c		89.9 ± 13.5
8d		674 ± 81
8e		433 ± 113

Table 1 (continued)

Compound	Structure	K _i (nM) ±SEM
8f		120 ± 14
8g		86.8 ± 6.9
8h		33.9 ± 3.7
8i		67.6 ± 8.1

where both the guanidinium and the 2-aminoimidazolium systems can establish IMHBs with the corresponding adjacent pyridine ring, (ii) compounds **8d-f** where only the 2-aminoimidazolium system can establish IMHB with the adjacent pyridine while the guanidinium system is free to rotate and interact with any residue in the binding site, and (iii) compounds **8g-i** where only the guanidinium cation can establish IMHB with the adjacent pyridine while the 2-aminoimidazolium system is free to rotate and interact with any residue in the binding site. Looking at the K_i values obtained for this family of compounds, it seems that the formation of an imidazolium-pyridine IMHB plus a guanidinium free to bind any residue in the binding site (compounds **8d-f**) is the most detrimental combination for target engagement (K_i values between 120 and 674 nM). On the contrary, the second best in terms of target engagement is the **8a-c** set (both guanidinium and imidazolium forming IMHBs) with K_i values between 89.9 and 138 nM. Finally, the best set in terms of binding is that which compounds can form a guanidinium-pyridine IMHB (**8g-i**) with K_i values between 33.9 and 86.8 nM. Therefore, it seems that the most relevant feature for target engagement, in this particular family of compounds, is the guanidinium-pyridine IMHB formation. However, if we compare the results of the **8g-i** set with those of the **7a-c** set (K_i between 0.8 and 12.3 nM) where both the guanidinium and 2-aminoimidazolium have free rotation and there is not competition between inter- and intra-molecular interactions, it could be concluded that, in general, the free rotation of the 2-aminoimidazolium system plays an important role in target engagement.

2.2.2. [³⁵S]GTPγS binding functional assays

Compounds which displayed K_i affinity values < 125 nM (compounds **7a-c**, **8c** and **8f-i**) were subjected to *in vitro* [³⁵S]GTPγS binding experiments in human PFC tissue to determine their nature as agonists or antagonists. As the α₂-AR is a member of the GPCR family, the direct evaluation of the degree of G-protein activation upon ligand binding can be made by determining guanine nucleotide exchange using radiolabelled GTPγS ([³⁵S]GTPγS) to observe agonist, antagonist or inverse agonist activity. Activation of the α₂-AR leads to the dissociation of GDP-Gα, followed by GDP-[³⁵S]GTPγS exchange, which can be used to measure the functional activity. Here, the phosphodiester bond that links the γ-phosphate to the rest of the nucleotide cannot be hydrolysed to reform GDP, and hence prevents the GTP binding protein from being inactivated, allowing for facile scintillation counting of the radiolabelled analogue.

In this experiment compounds **8c**, **8f**, **8g** and **8i** did not stimulate [³⁵S]GTPγS binding, which in principle is indicative of

antagonist functional activity. Interestingly, compounds **7a-c** and **8h** displayed agonist activity through the stimulation of GTP, but only at high concentrations. This did not correspond with the potent binding observed for these compounds, because a dose corresponding to the binding affinity would be expected to exert the corresponding activity.

Next, in order to confirm their α₂-AR functional activity, all compounds were subjected to another [³⁵S]GTPγS assay against the known α₂-AR agonist UK14304. Table 2 illustrates the antagonist effect induced by known α₂-AR antagonist RX821002 and compounds **7a-c**, **8c**, **8f-i** at a single concentration of 10⁻⁵ M on α₂-AR agonist UK14304's stimulation of [³⁵S]GTPγS binding. All of these compounds significantly induced an increase in the EC₅₀ of UK14304 by shifting the concentration-response curve to the right, which indicates competitive antagonism of the α₂-AR.

However, since derivatives **7a-c** and **8h** showed agonist properties in [³⁵S]GTPγS binding experiments, but antagonized the α₂-AR agonist UK14304 effect by increasing its EC₅₀ (Table 2), a third [³⁵S]GTPγS binding assay was performed in the presence or absence of the selective α₂-AR antagonist RX821002, to observe if the ligand stimulation of [³⁵S]GTPγS was occurring through α₂-ARs. As shown in Table 3, the stimulation of [³⁵S]GTPγS binding induced by compounds **7a**, **7b** and **7c** was blocked by RX821002, which suggests that these compounds are partial agonists of the α₂-AR as they stimulate [³⁵S]GTPγS binding by themselves but also antagonized the effect of a high-potency selective α₂-AR agonist as UK14304. Conversely, co-administration of RX821002 to compound **8h** resulted in no change in its stimulation of [³⁵S]GTPγS, clearly indicating that compound **8h** is acting as a potent α₂-AR antagonist, and that its stimulation of [³⁵S]GTPγS is perhaps the result of acting as an agonist at an alternative GPCR.

Table 2

EC₅₀ values (μM) obtained from the concentration-response curves for UK14304 (10⁻¹² to 10⁻³ M, 10 concentrations) stimulation of [³⁵S]GTPγS binding in the absence or presence of the different compounds (10⁻⁵ M).

Experiment	EC ₅₀ (μM) ±SEM	E _{max} (%) ±SEM
UK14304	1.77 ± 0.16	153 ± 4
UK14304 + RX821002	87.2 ± 7.5	98 ± 5
UK14304 + 7a	20.2 ± 0.4	110 ± 2
UK14304 + 7b	11.6 ± 3.0	155 ± 8
UK14304 + 7c	30.0 ± 1.5	171 ± 7
UK14304 + 8c	10.2 ± 0.3	127 ± 3
UK14304 + 8f	4.14 ± 0.33	139 ± 6
UK14304 + 8g	39.9 ± 3.2	140 ± 7
UK14304 + 8h	52.3 ± 1.9	96 ± 5
UK14304 + 8i	30.8 ± 2.8	122 ± 3

Table 3

EC₅₀ values (μM) obtained from the concentration-response curves for [³⁵S]GTPγS binding stimulation by compounds **7a**, **7b** and **7c** (10⁻¹² to 10⁻³ M, 10 concentrations) alone or in the presence of RX821002 (10⁻⁵ M).

Experiment	EC ₅₀ (μM) ±SEM	E _{max} (%) ±SEM
7a	18 ± 4	126 ± 3 ^a
7a + RX821002	64020 ± 44	122 ± 4
7b	534 ± 72	168 ± 4 ^a
7b + RX821002	2356 ± 107	130 ± 4
7c	46 ± 4	139 ± 18 ^a
7c + RX821002	487 ± 18	110 ± 11
8h	194 ± 21	149 ± 7 ^a
8h + RX821002	252 ± 27	154 ± 9

^a E_{max} represents the maximum [³⁵S]GTPγS binding stimulation induced by each compound over basal stimulation in the absence of the compound (100%).

2.3. Docking and molecular dynamics simulations

At the time of performing the present research, no crystal structure of any of the α₂-AR subtypes had been determined and thus, a homology model of the α_{2A}-AR (major subtype present in the PFC) was constructed in the Prime program of the Schrodinger suite [19], using a crystal structure of the β₂-AR as template (5JQH.pdb) [20], in order to carry out a docking study to understand the di-cationic structural activity observed and structure-affinity relationships of families **6**, **7** and **8**. Multiple conformers of compounds **6a-c**, **7a-f**, and **8a-i** were then docked into this model using Glide [21]. Docking resulted in two dominant poses for every compound, each with comparable scores. These poses are characterized by two electrostatic interactions: (i) that between one of the ligand's cationic groups (guanidinium or 2-aminoimidazolium) and D113^{3,32}, and (ii) another between the second ligand's cationic group and E94^{2,65} (superscript numbers denote the Ballesteros-Weinstein numbering scheme for Class A GPCRs [22]). The second salt-bridge formed by these compounds with the receptor could be driving their enhanced affinity relative to that of mono-cationic derivatives previously prepared by us [10–15]. Further, position 2.65 is a glutamate in all α-AR, but not in β-AR, providing a potential route to selectively targeting α-AR. It should also be noted that position 2.65 is a glutamate in all dopamine receptors, but no in 5-HT receptors [23].

Molecular dynamics (MD) simulations were next carried out to determine the stability of these poses and the likelihood for prevalence of one over the other that would facilitate structure-based drug design (see examples in Fig. 3, Figs. S1 and S2, ESI). In general, compounds with low α₂-AR affinity (e.g. **6a**, K_i = 355 nM, in Figs. S1 and S2, ESI), despite remaining stably bound to D113 in the orthosteric binding pocket throughout simulation, show strong fluctuations due to instability caused by solvent exposure, which disrupts the ionic interaction with E94. However, high α₂-AR affinity compounds (e.g. **7a**, **7b** and **7c**, K_i = 12.30, 1.77 and 0.82 nM, respectively; in Figs. S1 and S2, ESI) remain in a stable pose throughout simulation. Analysis of interactions with key Serine residues on TM5 S200^{5,42} and S204^{5,46} could also shed light on which molecules would have agonist or antagonist functional activity. While both poses are relatively stable throughout simulation, differences emerge. The pose in which the di-substituted arylguanidinium forms a hydrogen bond (HB) with D113^{3,32} (Pose A), places the substituent (alkyl, furan-2-yl) to fill the pocket formed adjacent to TM5, while the other cationic group extends towards the extracellular solvent to interact with E94^{2,65} (Fig. 3a, showing compound **8h**, K_i = 33.9 nM).

When the cationic groups are in the opposite orientation (Pose B), the pocket at TM5 is left vacant. This is likely unfavorable as

residues on TM5 are known to be important for endogenous ligand-binding as well as many discovered adrenoceptor ligands, particularly S200^{5,42} and S204^{5,46} which likely form HBs with noradrenaline [24]. Furthermore, in Pose B, water molecules fill this particular pocket, which would be detrimental to the affinity of molecules were this to be the correct pose. Thus, Pose A is predicted to be the orientation in which compounds bind to the receptor which fills the pocket at TM5. It also follows that molecules which do not engage with key residues on TM5 S200^{5,42} or S204^{5,46} are likely to act as antagonists which do not activate the receptor.

These simulations were used to give some insight into the results observed for our lead compounds **7a-c** and **8h**. Experimentally, we have observed that the affinity of di-substituted guanidiniums is higher than that of the mono-substituted analogues and, as the simulation results suggest, this indicates that they interact with the endogenous binding site adjacent to TM5. The partial agonism of compounds **7a**, **7b** and **7c** can be rationalized by their proximity to the S200 and S204 in TM5. As for their pyridine analogues, **8b-c** and **8h-i**, which show no partial agonism, an IMHB between the pyridine N and guanidinium NH is maintained throughout simulation and prevents the alkyl/furan-2-yl substituent from extending as close to TM5, seemingly conferring antagonist activity to these compounds (Fig. S3, ESI).

By December 2019, four crystal structures of the different α₂-AR subtypes have been subsequently deposited in the PDB: the crystal structure of the human α_{2A}-AR in complex with a partial agonist (PDB: 6KUY [25]); that of the α_{2A}-AR receptor of the Spodoptera frugiperda in complex with an antagonist (PDB: 6KUX [26]), that of the human α_{2C}-AR with an antagonist (PDB: 6KUW [27]) and also the structure of the Spodoptera frugiperda α_{2B}-AR in complex with GoA (PDB: 6K41 [28]). Accordingly, we have carried out computational studies to validate the results we obtained with the α_{2A}-AR homology model structure. Thus, we have docked compound **8h**, as a model of the compounds here studied, in the 6KUY, 6KUX and 6KUW crystal structures, which correspond to the two most important adrenoceptor subtypes in the brain's PFC (α_{2A}- and α_{2C}-). When docking **8h** into the α_{2A}-AR structures (6KUX and 6KUY; Figs. S4 and S5, respectively) we observed the same interactions (mostly with E94 and D113) that we had seen in the docking of **8h** into the α_{2A}-AR homology model developed by us. In the case of docking **8h** into the α_{2C}-AR structure (6KUW, Fig. S6) some different contacts are observed, but the interactions established are still favorable for binding. Finally, we have superposed the 'best pose' obtained for **8h** within our α_{2A}-AR homology model and the 'best poses' obtained with 6KUX and 6KUY and we observed a very good alignment (RMSD = 1.66 and 2.09, respectively; see Fig. 4).

All the molecular modelling studies provide a possible rationale for the pharmacological results observed for high affinity partial agonists/antagonists, **7a-c** and **8h**. Compounds with di-substituted guanidines where one of these substituents have been optimized to take advantage of the pocket adjacent to TM5 without engaging S200^{5,42} or S204^{5,46} are desirable, while di-substituted 2-aminoimidazolines may also be considered. Moreover, the presence of an additional mono-substituted cationic group is favorable to interact with E94^{2,65}, as there is little room for second substituents and they tend to extend into solvent.

3. Conclusions

Aiming to obtain compounds with excellent receptor engagement, while displaying selective blockade at the α₂-AR, we have prepared a series of di-aryl (di-phenyl, phenyl/pyridin-2-yl or di-pyridin-2-yl) mono- or di-substituted guanidines and 2-aminoimidazolines emanating from previous encouraging results. Following different synthetic strategies three disubstituted bis-

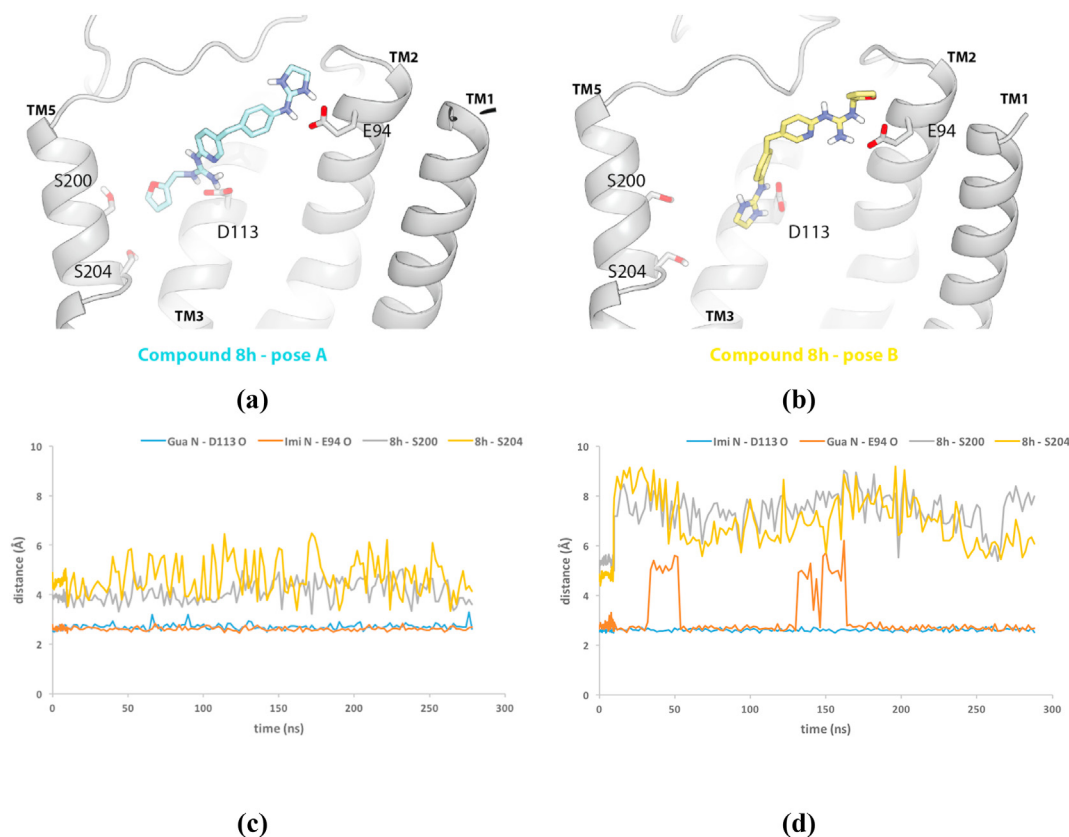


Fig. 3. Representative simulation snapshots of (a) Pose A demonstrated for compound **8h**. The di-substituted guanidinium interacts with D113 and extends to fill the pocket formed at TM5, the 2-aminoimidazolium interacts with E94, (b) Pose B demonstrated for compound **8h**. The 2-aminoimidazolium interacts with D113, leaving the TM5 pocket vacant, the di-substituted guanidinium interacts with E94, placing the furan-2-yl substituent towards solvent. (c) In pose A both salt bridges are stable and the binding pocket at TM5 is filled by the ligand, whereas (d) in pose B the salt bridge to E94 is less stable due to solvent exposure of the furan-2-yl substituent and the binding pocket at TM5 is left vacant.



Fig. 4. Alignment of the docked 'best-pose' of compound **8h** in the in-house α_{2A} -AR homology model and that in the 6KUX (α_{2A} -AR, RMSD = 1.66) crystal structure (left) or that in the 6KUY (α_{2A} -AR, RMSD = 2.09) crystal structure (right).

guanidines with a di-phenylmethane core were prepared as well as fifteen hybrid guanidine/2-aminoimidazoline derivatives with di-phenylmethane (three), di-phenylethane (three), di-pyridin-2-ylmethane (three), and benzylpyridin-2-yl (six) cores.

Additionally, the *in vitro* α_{2A} -AR binding affinity of all the compounds prepared was studied in human PFC brain tissue. Despite

the α_{2A} -AR being the predominant subtype in the human PFC, a reduced presence of the α_{2C} -AR is also acknowledged. Thus, we cannot exclude a minimal incidence of this minority subtype in the results shown. Thus, we found that the presence of a phenyl-2-aminoimidazolium cation, a CH_2 linker between the aryl systems and the steric extension at the aryl-guanidinium contribute to

achieve good α_2 -AR engagement ($K_i < 68$ nM). Furthermore, even though formation of an IMHB increases α_2 -AR affinity in pyridin-2-yl-guanidine compounds, in general, the free rotation of a 2-aminoimidazolium system attached to the diaryl core plays an even more important role in target engagement.

Compounds **7a-c**, **8c** and **8f-i**, which displayed α_2 -AR K_i affinity values < 125 nM, were assessed as agonists or antagonists *in vitro* via [35 S]GTP γ S functional binding experiments in PFC tissue. Since the results were not conclusive, all compounds were subjected to an alternate [35 S]GTP γ S assay against UK14304 (known selective α_2 -AR agonist) to elucidate their functional activity. Considering that derivatives **7a-c** and **8h** showed agonist properties by themselves in [35 S]GTP γ S binding experiments, but increased the EC $_{50}$ of UK14304, a third [35 S]GTP γ S binding assay was performed in the presence of RX821001 (selective α_2 -AR antagonist). This assay indicated that the stimulation of [35 S]GTP γ S binding induced by **7a**, **7b** and **7c** was blocked by RX821001, suggesting α_2 -AR partial agonism, whereas lack of change in RX821001 stimulation of [35 S]GTP γ S when co-administered with **8h** indicates potent α_2 -AR antagonism.

Finally, computational studies (docking and MD in an in-house α_{2A} -AR homology model) have thrown light to the pharmacological results observed for high affinity partial agonists/antagonists, **7a-c** and **8h**. These studies suggest that antagonism is achieved by diarylmethane derivatives with a di-substituted guanidine which substituent occupy the pocket adjacent to TM5 without engaging S200^{5,42} or S204^{5,46}, and a mono-substituted cationic group, which favorably interact with E94^{2,65}, as there is little room for second substituents and they tend to extend into solvent. Comparative docking studies with our own α_{2A} -AR homology model and the recently reported crystal structures of α_{2A} -AR (complexed with a partial agonist or an antagonist) and α_{2C} -AR, showed similar results.

Summarizing, we not only have found a new antagonist with excellent α_2 -AR receptor engagement, but also we have determined the structural features that will result in optimal target engagement. All this will allow us designing novel therapeutics to treat depression (some of our previous compounds have already shown to reach the brain of rats in *in vivo* microdialysis experiments and exhibited anti-stress activities in animal tests [11,29]).

4. Experimental

4.1. Pharmacology

4.1.1. Preparation of membranes

Neural membranes (P2 fractions) were prepared from the PFC of human brains obtained at autopsy in the Basque Institute of Legal Medicine, Bilbao, Spain. Post-mortem human brain samples of each subject (~1 g) were homogenized using a Teflon-glass grinder (10 up-and-down strokes at 1500 rpm) in 10 vol of homogenization buffer (5 mM Tris-HCl and 0.25 M sucrose, pH 7.4). The crude homogenate was centrifuged for 5 min at 1000 g (4 °C), and the supernatant was centrifuged again for 10 min at 40,000 g (4 °C). The resultant pellet was washed twice in 5 vol of resuspension buffer (50 mM Tris-HCl, pH 7.5) and re-centrifuged in similar conditions. Aliquots of 2 mg protein were stored at -70 °C until assay. Protein concentration was measured according to the Bradford method, using bovine serum albumin as standard.

4.1.2. [3 H]RX821002 binding assays

Specific [3 H]RX821002 binding was measured in 0.25 mL aliquots (50 mM Tris-HCl, pH 7.5) of the human brain membranes, which were incubated in 96-well plates with [3 H]RX821002 (2 nM) for 30 min at 25 °C in the absence or presence of the competing compounds (10^{-12} to 10^{-3} M, 10 concentrations). Incubations were

terminated by separating free ligand from bound ligand by rapid filtration under vacuum (1450 Filter Mate Harvester, PerkinElmer) through GF/C glass fiber filters. The filters were then rinsed three times with 300 μ L binding buffer, air-dried (120 min), and counted for radioactivity by liquid scintillation spectrometry using a MicroBeta TriLux counter (PerkinElmer). Specific binding was determined and plotted as a function of the compound concentration. Nonspecific binding was determined in the presence of idazoxan (10^{-3} M). Analysis of competition experiments to obtain the inhibition constant (K_i) were performed by non-linear regression using the Graph Pad Prism 5 program. All experiments were analysed assuming a one-site model of radioligand binding.

4.1.3. [35 S]GTP γ S binding assays

The incubation buffer for measuring [35 S]GTP γ S binding to brain membranes contained, in a total volume of 250 μ L, 1 mM EGTA, 3 mM MgCl $_2$, 100 mM NaCl, 50 mM GDP, 50 mM Tris-HCl at pH 7.4, and 0.5 nM [35 S]GTP γ S. Protein aliquots were thawed and resuspended in the same buffer. The incubation was started by addition of the membrane suspension (20 μ g of membrane proteins *per well*) to the previous mixture and was performed at 30 °C for 120 min, with shaking. In order to evaluate the influence of the compounds on [35 S]GTP γ S binding, ten concentrations (10^{-12} to 10^{-3} M) of the different compounds were added to the assay. Incubations were terminated by separating free ligand from bound ligand by rapid filtration under vacuum (1450 Filter Mate Harvester, PerkinElmer) through GF/C glass fiber filters. The filters were then rinsed three times with 300 μ L of ice-cold incubation buffer and air-dried (90 min). The radioactivity trapped was determined by liquid scintillation spectrometry (MicroBeta TriLux counter, PerkinElmer). The [35 S]GTP γ S bound was about 6–15% of the total [35 S]GTP γ S added. Nonspecific binding of the radioligand was defined as the remaining [35 S]GTP γ S binding in the presence of 10 μ M unlabelled GTP γ S. E $_{max}$ represents the maximum [35 S]GTP γ S binding stimulation over basal.

4.2. Computational

4.2.1. Homology modelling and docking

A homology model of the α_2 -AR was constructed as described in previous studies [15]. Briefly, we used the Modeller 9.12 software [30] to construct homology models of the human α_{2A} -AR using sequences from www.uniprot.org (α_{2A} AR, P08913), based on three template structures of the homologous β_2 -adrenoceptor (PDB IDs: β_2 -AR; 2R4S, 3D4S, and 3SN6), which has 38.9% homology with the α_{2A} -AR and 35.2% homology with the α_{2C} -AR. Molecules were prepared in the Maestro software and docked using Glide. Poses for simulation were chosen based on those that incorporated ionic interaction with D113^{3,32}, which is known to be important to GPCR-binding ligands, and a second ionic interaction between the ligand and E94^{2,65}.

Additionally, the structures of the α_{2A} -AR complexed with a partial agonist (6KUY) or with an antagonist (6KUX) as well as that of the α_{2C} -AR complexed with an antagonist were retrieved from the RCSB PDB to be used for docking studies.

4.2.2. System setup for molecular dynamics (MD) simulations

MD simulations of the α_2 -AR were based on complexes formed from docking compounds **6a-6c**, **7a-7f**, **8a-8i** to the constructed homology model. Two poses (one with each cationic group in contact with D113^{3,32}/E94^{2,65}) were simulated for these 18 compounds, resulting in a total of 36 simulations. Each simulation was ~250 ns in length, for a total of 9 μ s. For each complex, hydrogen atoms were added using Prime (Schrödinger Inc.), and protein chain termini were capped with the neutral groups acetyl and

methanamide. Titratable residues were left in their dominant protonation state at pH 7.0. All aspartate residues were deprotonated, as is expected in the inactive state of GPCRs to which antagonists bind. Both guanidinium/2-amino-imidazolium groups were positively charged. The prepared protein structures were aligned on the transmembrane helices to the Orientation of Proteins in Membranes (OPM) [31] structure of PDB 5JQH, and internal waters added with Dowser [32]. The structures were then inserted into a pre-equilibrated palmitoyl-oleoyl-phosphatidylcholine (POPC) bilayer and solvated with 0.15 M NaCl in explicitly represented water, then neutralized by removing sodium ions.

We used the CHARMM36 parameter set for protein molecules, lipid molecules, and salt ions, and the CHARMM TIP3P model for water; protein parameters incorporated CMAP terms [33]. Parameters for ligands were generated using the CHARMM General Force Field (CGenFF [34]) with the ParamChem server (paramchem.org), version 1.0.0. Hydrogen mass repartitioning was employed to enable a timestep of 4.0 fs [35].

Simulations were performed on GPUs using the CUDA version of PMEMD (Particle Mesh Ewald Molecular Dynamics) in Amber15 [36]. Prepared systems were minimized, then equilibrated as follows: the system was heated using the Langevin thermostat from 0 to 100 K in the NVT ensemble over 12.5 ps with harmonic restraints of 10.0 kcal mol⁻¹ Å⁻² on the non-hydrogen atoms of lipid, protein and ligand, and initial velocities sampled from the Boltzmann distribution. The system was then heated to 310 K over 125 ps in the NPT ensemble with semi-isotropic pressure coupling and a pressure of 1 bar. Further equilibration was performed at 310 K with harmonic restraints on the protein and ligand starting at 5.0 kcal mol⁻¹ Å⁻² and reduced by 1.0 kcal mol⁻¹ Å⁻² in a stepwise fashion every 2 ns, for a total of 10 ns of additional restrained equilibration. Simulations were conducted in the NPT ensemble at 310 K and 1 bar, using a Langevin thermostat and Monte Carlo barostat. In each of these simulations, we performed 5 ns of unrestrained equilibration followed by a production run of 250 ns. Simulations used periodic boundary conditions, and a time step of 4.0 fs. Bond lengths to hydrogen atoms were constrained using SHAKE. Non-bonded interactions were cut off at 9.0 Å, and long-range electrostatic interactions were computed using the particle mesh Ewald (PME) method with an Ewald coefficient β of approximately 0.31 Å and B-spline interpolation of order 4. The FFT grid size was chosen such that the width of a grid cell was approximately 1 Å.

Trajectory snapshots were saved every 100 ps during production simulations. Trajectory analysis was performed using VMD [37] and CPPTRAJ [38], and visualization was performed using VMD. Two metrics were used to determine ligand stability in their respective poses: the distance between each cationic group of the ligand and either D113^{3.32} or E94^{2.65}. Figures were rendered using PyMol [39].

4.3. Synthesis

All commercial chemicals were obtained from Sigma-Aldrich or Fluka and used without further purification. Deuterated solvents for NMR use were purchased from Apollo. Dry solvents were prepared using standard procedures, according to Vogel [40], with distillation prior to use. Solvents for synthesis purposes were used at GPR grade. Analytical TLC was performed using Merck Kieselgel 60 F254 silica gel plates or Polygram Alox N/UV254 aluminium oxide plates. Visualization was by UV light (254 nm). NMR spectra were recorded on Bruker DPX-400 Avance spectrometers, operating at 400.13 MHz and 600.1 MHz for ¹H NMR; 100.6 MHz and 150.9 MHz for ¹³C NMR. Shifts are referenced to the internal solvent signals. NMR data were processed using Bruker TOPSPIN software. HRMS spectra were measured on a Micromass LCT electrospray TOF

instrument with a WATERS 2690 autosampler and methanol/acetonitrile as carrier solvent. Melting points were determined using a Stuart Scientific Melting Point SMP1 apparatus and are uncorrected. Infrared spectra were recorded on a PerkinElmer Spectrum One FT-IR Spectrometer equipped with a Universal ATR sampling accessory. HPLC purity analysis was carried out using a Varian ProStar system equipped with a Varian Prostar 335 diode array detector and a manual injector (20 µL). For purity assessment, UV detection was performed at 245 nm and peak purity was confirmed using a purity channel. The stationary phase consisted of an ACE 5C18-AR column (150 × 4.6 mm), and the mobile phase used the following gradient system, eluting at 1 mL/min: aqueous formate buffer (30 mM, pH 3.0) for 10 min, linear ramp to 85% methanol buffered with the same system over 25 min, hold at 85% buffered methanol for 10 min. Minimum requirement for purity was set at 95%.

4.3.1. General methods

4.3.1.1. Method A: generation of guanidine hydrochlorides from *N*-(*tert*-butoxycarbonyl) protected guanidine and iminoimidazolidine derivatives using hydrochloric acid in 1,4-dioxane. To the starting Boc-protected guanidine was added 4 M HCl/dioxane (6.0 eq. per Boc group) and a 1:1 solution of ¹PrOH:CH₂Cl₂, such as to maintain a reaction concentration of 0.2 M. The mixture was stirred at 55 °C for 3–4 h, after which all starting material was consumed as adjudged by TLC analysis. Solvent and excess HCl were then removed under vacuum and the crude salt was dissolved in a minimum volume of H₂O. It was washed with CH₂Cl₂ (2 × 5 mL) and then purified using reverse phase chromatography (C-8 silica) using 100% H₂O as mobile phase.

4.3.2. Characterization of final salts

4.3.2.1. 4,4'-Di[3-(*furanyl*-2-methyl)guanidino]diphenylmethane dihydrochloride (6a). Following **Method A**, to a solution of 4 M HCl/1,4-dioxane (12.0 eq., 600 µL, 2.28 mmol) was added compound **17a** (1.0 eq., 120 mg, 0.19 mmol) affording the title compound (89 mg, 91%) as yellow solid. Mp: 135–139 °C. δ_{H} (400 MHz, D₂O): 3.90 (s, 2H, CH₂), 4.34 (s, 4H, CH₂), 6.21 (app. t, 2H, *J* = 4.0, Ar), 6.32 (app. t, 2H, *J* = 4.0, Ar), 7.08 (d, 4H, *J* = 8.2, Ar), 7.23 (d, 4H, *J* = 8.2, Ar), 7.38 (app. t, 2H, *J* = 4.0, Ar). δ_{C} (125 MHz, D₂O): 38.1 (CH₂), 48.7 (CH₂), 107.1 (CH Ar), 110.3 (CH Ar), 126.3 (CH Ar), 130.1 (CH Ar), 132.1 (qC Ar), 141.1 (qC Ar), 143.3 (CH Ar), 149.1 (qC Ar), 155.3 (qC CN). ν_{max} (ATR)/cm⁻¹: 3134 (NH), 2929, 1626, 1609, 1437, 1343, 1073, 1017, 975. HRMS: (*m/z* ES⁺): Found: 443.2190 (M⁺ + H, C₂₅H₂₇N₆O₂ Requires: 443.2193). Purity by HPLC: 98.4% (*t_r* 23.63 min).

4.3.2.2. 4,4'-Di[3-(*hydroxyethyl*)guanidino]diphenylmethane dihydrochloride (6b). Following **Method A**, to a solution of 1.25 M HCl/CH₃OH (15.0 eq., 4.56 mL, 5.7 mmol) was added compound **17b** (1.0 eq., 250 mg, 0.38 mmol) affording the title compound as a yellow gum (148 mg, 88%). δ_{H} (400 MHz, D₂O): 3.25 (t, 4H, *J* = 8.0, CH₂), 3.57 (t, 4H, *J* = 8.0, CH₂), 3.83 (s, 2H, CH₂), 7.05 (d, 4H, *J* = 8.0, Ar), 7.17 (d, 4H, *J* = 8.0, Ar). δ_{C} (125 MHz, D₂O): 40.1 (CH₂), 42.6 (CH₂), 59.8 (CH₂), 125.9 (CH Ar), 130.1 (CH Ar), 132.2 (qC Ar), 140.9 (qC Ar), 155.7 (qC CN). ν_{max} (ATR)/cm⁻¹: 3319 (NH), 3161 (NH), 2963, 1600, 1622, 1514, 1351, 1248, 1061, 1019, 920. HRMS: (*m/z* ES⁺): Found: 371.2190 (M⁺ + H, C₁₉H₂₇N₆O₂ Requires: 371.2199). Purity by HPLC: 95.5% (*t_r* 19.95 min).

4.3.2.3. 4,4'-Di[3-(*propyl*)guanidino]diphenylmethane dihydrochloride (6c). Following **Method A**, to a solution of 4 M HCl/1,4-dioxane (12.0 eq., 1.55 mL, 6.12 mmol) was added compound **17c** (1.0 eq., 290 mg, 0.51 mmol) affording the title compound as a yellow solid (199 mg, 89%). Mp: 144–150 °C. δ_{H} (400 MHz, D₂O): 0.79 (t, 6H, *J* = 8.0, CH₃), 1.46 (m, 4H, CH₂), 3.07 (t, 4H, *J* = 8.0, CH₂),

3.83 (s, 2H, CH₂), 7.08 (d, 4H, *J* = 8.1, Ar), 7.21 (d, 4H, *J* = 8.1, Ar). δ_C (125 MHz, D₂O): 10.2 (CH₃), 21.2 (CH₂), 39.8 (CH₂), 43.1 (CH₂), 126.1 (CH Ar), 130.1 (CH Ar), 132.3 (qC Ar), 140.9 (qC Ar), 155.7 (qC CN). ν_{\max} (ATR)/cm⁻¹: 3129 (NH), 2934, 1625, 1599, 1511, 1296, 1246, 1147, 1048, 805. HRMS: (*m/z* ESI⁺): Found: 367.2605 (M⁺ + H, C₂₁H₃₁N₆ Requires: 367.2605). Purity by HPLC: 98.3% (t_R 24.60 min).

4.3.2.4. 4-Guanidino-4'-(2-aminoimidazoline)diphenylmethane dihydrochloride (7a). Following **Method A**, to a solution of 4 M HCl/1,4-dioxane (24.0 eq., 850 μ L, 3.36 mmol) was added compound **19a** (1.0 eq., 100 mg, 0.14 mmol) affording the title compound as a yellow solid (52 mg, 98%). Mp: 219–221 °C decomposed. δ_H (400 MHz, D₂O): 3.59 (s, 4H, CH₂), 3.88 (s, 2H, CH₂), 7.08 (m, 4H, H-2', Ar), 7.22 (m, 4H, Ar). δ_C (100 MHz, D₂O): 40.4 (CH₂), 42.6 (CH₂), 124.6 (CH Ar), 126.3 (CH Ar), 130.0 (CH Ar), 130.1 (CH Ar), 132.1 (qC Ar), 133.5 (qC Ar), 140.6 (qC Ar), 144.6 (qC Ar), 156.3 (qC CN), 158.7 (qC CN). ν_{\max} (ATR)/cm⁻¹: 3384 (NH), 3270 (NH), 2993, 1602, 1518, 1406, 1232, 1147, 801. HRMS: (*m/z* ESI⁺): Found: 309.1826 (M⁺ + H, C₁₇H₂₁N₆ Requires: 309.1822). Purity by HPLC: 97.6% (t_R 19.91 min).

4.3.2.5. 4-(2-Aminoimidazolino)-4'-[3-(furanlyl-2-methyl)guanidino]diphenylmethane dihydrochloride (7b). Following **Method A**, to a solution of 4 M HCl/1,4-dioxane (18.0 eq., 1.30 mL, 5.4 mmol) was added compound **19b** (1.0 eq., 200 mg, 0.30 mmol) affording the title compound as a white solid (111 mg, 80%). Mp: 201–206 °C decomposed. δ_H (400 MHz, D₂O): 3.75 (s, 4H, CH₂), 4.03 (s, 2H, CH₂), 4.50 (s, 2H, CH₂), 6.44 (d, 1H, *J* = 4.0, Ar), 6.47 (t, 1H, *J* = 4.0, Ar), 7.22 (d, 4H, *J* = 8.3, Ar), 7.36 (d, 4H, *J* = 8.3, Ar), 7.34 (br s, 1H, Ar). δ_C (100 MHz, D₂O): 38.0 (CH₂), 40.0 (CH₂), 42.6 (CH₂), 108.7 (CH Ar), 110.7 (CH Ar), 124.8 (CH Ar), 126.4 (CH Ar), 130.2 (CH Ar), 130.5 (CH Ar), 132.3 (qC Ar), 133.3 (qC Ar), 140.8 (qC Ar), 141.4 (qC Ar), 143.3 (CH Ar), 149.2 (qC Ar), 155.5 (qC CN), 158.6 (qC CN). ν_{\max} (ATR)/cm⁻¹: 3140 (NH), 2981, 1647, 1570, 1387, 1244, 1096, 1022, 975. HRMS: (*m/z* ESI⁺): Found: 389.2084 (M⁺ + H, C₂₂H₂₅N₆O Requires: 389.2094). Purity by HPLC: 95.1% (t_R 23.44 min).

4.3.2.6. 4-[3-(Propyl)guanidino]-4'-(2-aminoimidazolino)diphenylmethane dihydrochloride (7c). Following **Method A**, to a solution of 4 M HCl/1,4-dioxane (18.0 eq., 1.40 mL, 5.58 mmol) was added compound **19c** (1.0 eq., 200 mg, 0.31 mmol) affording the title compound as a brown solid (126 mg, 96%). Mp: 221–225 °C decomposed. δ_H (400 MHz, D₂O): 0.78 (t, 3H, *J* = 8.3, CH₃), 1.45 (m, 2H, CH₂), 3.07 (t, 2H, *J* = 8.3, CH₂), 3.59 (s, 4H, CH₂), 3.87 (s, 2H, CH₂), 7.06 (d, 4H, *J* = 8.1, Ar), 7.2 (d, 4H, *J* = 8.1, Ar). δ_C (100 MHz, D₂O): 10.3 (CH₃), 21.4 (CH₂), 40.0 (CH₂), 42.6 (CH₂), 43.0 (CH₂), 124.6 (CH Ar), 126.2 (CH Ar), 130.0 (CH Ar), 130.1 (CH Ar), 132.3 (qC Ar), 133.0 (qC Ar), 140.7 (qC Ar), 141.0 (qC Ar), 155.2 (qC CN), 158.7 (qC CN). ν_{\max} (ATR)/cm⁻¹: 3159 (NH), 2968, 1717, 1650, 1592, 1485, 1468, 1284, 1240, 1088, 1018, 820, 758. HRMS: (*m/z* ESI⁺): Found: 351.2292 (M⁺ + H, C₂₀H₂₇N₆ Requires: 351.2292). Purity by HPLC: 99.7% (t_R 22.49 min).

4.3.2.7. [4-Guanidino-4'-(2-aminoimidazolino)]-1,2-diphenylethane dihydrochloride (7d). Following **Method A**, to a solution of 4 M HCl/1,4-dioxane (24.0 eq., 1.24 mL, 5.04 mmol) was added compound **19d** (1.0 eq., 150 mg, 0.21 mmol) affording the title compound as a yellow solid (71 mg, 86%). Mp: 210–215 °C decomposed. δ_H (400 MHz, D₂O): 2.83 (s, 4H, CH₂), 3.58 (s, 4H, CH₂), 7.03 (m, 4H, Ar), 7.18 (m, 4H, Ar). δ_C (125 MHz, D₂O): 35.8 (CH₂), 35.8 (CH₂), 42.6 (CH₂), 124.1 (CH Ar), 125.7 (CH Ar), 129.6 (CH Ar), 129.9 (CH Ar), 131.7 (qC Ar), 132.7 (qC Ar), 140.5 (qC Ar), 141.5 (qC Ar), 156.2 (qC CN), 158.6 (qC CN). ν_{\max} (ATR)/cm⁻¹: 3135 (NH), 2986, 1648, 1608, 1578, 1512, 149, 1255, 1019, 827. HRMS: (*m/z* ESI⁺): Found: 323.1977 (M⁺ + H, C₁₈H₂₃N₆ Requires: 323.1987). Purity by HPLC: 97.9% (t_R 21.29 min).

4.3.2.8. [4-(2-Aminoimidazolino)-4'-[3-(furanlyl-2-methyl)guanidino]]-1,2-diphenylethane dihydrochloride (7e). Following **Method A**, to a solution of 4 M HCl/1,4-dioxane (18.0 eq., 540 μ L, 2.16 mmol) was added compound **19e** (1.0 eq., 80 mg, 0.12 mmol) affording the title compound as a yellow solid (57 mg, 82%). Mp: 237–240 °C decomposed. δ_H (400 MHz, D₂O): 2.86 (br s, 4H, CH₂), 3.59 (br s, 4H, CH₂), 4.34 (s, 2H, CH₂), 6.28 (m, 1H, Ar), 6.32 (m, 1H, Ar), 7.04 (m, 4H, Ar), 7.39 (m, 4H, Ar), 7.39 (br s, 1H, Ar). δ_C (100 MHz, D₂O): 35.8 (CH₂), 38.0 (CH₂), 42.6 (CH₂), 108.1 (CH Ar), 110.9 (CH Ar), 124.3 (CH Ar), 125.9 (CH Ar), 129.8 (CH Ar), 130.0 (CH Ar), 131.7 (qC Ar), 132.2 (qC Ar), 141.0 (qC Ar), 141.5 (qC Ar), 143.2 (CH Ar), 149.1 (qC Ar), 155.4 (qC CN), 158.7 (qC CN). ν_{\max} (ATR)/cm⁻¹: 3143 (NH), 2892, 1648, 1602, 1612, 1461, 1381, 1345, 1240, 1148, 1084, 1016, 825. HRMS: (*m/z* ESI⁺): Found: 403.2240 (M⁺ + H, C₂₃H₂₇N₆O Requires: 403.2240). Purity by HPLC: 96.6% (t_R 24.16 min).

4.3.2.9. [4-[3-(Propyl)guanidino]-4'-(2-aminoimidazolino)]-1,2-diphenylethane dihydrochloride (7f). Following **Method A**, to a solution of 4 M HCl/1,4-dioxane (18.0 eq., 890 μ L, 3.6 mmol) was added compound **19f** (1.0 eq., 130 mg, 0.20 mmol) affording the title compound as a yellow solid (80 mg, 91%). Mp: 271–275 °C decomposed. δ_H (400 MHz, D₂O): 0.79 (t, 3H, *J* = 7.4, CH₃), 1.46 (m, 2H, CH₂), 2.82 (br s, 4H, CH₂), 3.07 (t, 2H, *J* = 7.4, CH₂), 3.59 (br s, 4H, CH₂), 7.02 (d, 4H, *J* = 8.3, Ar), 7.11 (d, 4H, *J* = 8.3, Ar). δ_C (100 MHz, D₂O): 10.2 (CH₃), 21.4 (CH₂), 35.8 (2 CH₂), 42.6 (CH₂), 43.0 (CH₂), 124.1 (CH Ar), 125.8 (CH Ar), 129.8 (CH Ar), 129.9 (CH Ar), 132.0 (qC Ar), 132.7 (qC Ar), 140.9 (qC Ar), 141.3 (qC Ar), 155.1 (qC CN), 158.6 (qC CN). ν_{\max} (ATR)/cm⁻¹: 3018 (NH), 2849, 1593, 1508, 1355, 1234, 1144, 1081, 1017, 826. HRMS: (*m/z* ESI⁺): Found: 365.2305 (M⁺ + H, C₂₁H₂₉N₆ Requires: 365.2296). Purity by HPLC: 95.1% (t_R 23.01 min).

4.3.2.10. 6-(2-Aminoimidazolino)-6'-(guanidino)dipyridinyl-3-methane dihydrochloride (8a). Following **Method A**, to a solution of 4 M HCl/1,4-dioxane (24.0 eq., 840 μ L, 3.36 mmol) was added compound **19g** (1.0 eq., 100 mg, 0.14 mmol) affording the title compound as a yellow solid (49 mg, 92%). Mp: 149–151 °C decomposed. δ_H (400 MHz, D₂O): 3.64 (s, 2H, CH₂), 3.67 (s, 4H, CH₂), 6.74 (d, 2H, *J* = 8.1, H-3', H-3), 7.45 (dd, 2H, ³*J* = 8.1, ⁴*J* = 2.2, H-4', H-4), 7.99 (d, 2H, ⁴*J* = 2.1, H-6', H-6). δ_C (100 MHz, D₂O): 33.4 (CH₂), 42.0 (CH₂-Imid), 112.6 (CH, Ar-3'), 113.3 (CH, Ar-3'), 131.9 (q, Ar-5', Ar-5'), 139.7 (CH, Ar-4, Ar-4'), 146.0 (CH, Ar-6'), 146.5 (CH, Ar-6), 148.8 (q, Ar-2' or Ar-2), 149.8 (q, Ar-2 or Ar-2'), 154.6 (q, C=N), 156.3 (q, C=N). ν_{\max} (ATR)/cm⁻¹: 3185 (NH), 2980, 1624, 1600, 1481, 1355, 1242, 1027, 965. HRMS: (*m/z* ESI⁺): Found: 311.1728 (M⁺ + H, C₁₅H₁₉N₈ Requires: 311.1733). Purity by HPLC: 98.4% (t_R 1.75 min).

4.3.2.11. 6-(2-Aminoimidazolino)-6'-[2-(furanlyl-2-methyl)guanidino]dipyridinyl-3-methane dihydrochloride (8b). Following **Method A**, to a solution of 4 M HCl/1,4-dioxane (18.0 eq., 400 μ L, 1.62 mmol) was added compound **19h** (1.0 eq., 64 mg, 0.09 mmol) affording the title compound as a yellow solid (34 mg, 82%). Mp: 164–167 °C decomposed. δ_H (400 MHz, D₂O): 3.76 (s, 2H, CH₂), 3.79 (s, 4H, CH₂), 4.54 (s, 2H, CH₂), 6.44 (br s, 2H, Ar), 6.91 (m, 2H, Ar), 7.51 (br s, 1H, Ar), 7.51 (dd, 1H, ³*J* = 8.1, ⁴*J* = 2.4, Ar), 7.61 (dd, 1H, ³*J* = 8.1, ⁴*J* = 2.4, Ar), 7.96 (s, 1H, Ar), 8.11 (s, 1H, Ar). δ_C (100 MHz, D₂O): 33.7 (CH₂), 37.8 (CH₂), 42.2 (CH₂), 108.5 (CH Ar), 110.6 (CH Ar), 112.5 (CH Ar), 113.2 (CH Ar), 128.7 (qC Ar), 130.6 (qC Ar), 139.6 (CH Ar), 139.8 (CH Ar), 143.3 (CH Ar), 145.5 (CH Ar), 146.5 (CH Ar), 148.5 (qC Ar), 149.5 (qC Ar), 149.5 (qC Ar), 153.7 (qC CN), 156.0 (qC CN). ν_{\max} (ATR)/cm⁻¹: 3127 (NH), 2918, 2894, 1629, 1601, 1574, 1388, 1281, 1234, 1045, 1025, 828, 741. HRMS: (*m/z* ESI⁺): Found: 391.1993 (M⁺ + H, C₂₀H₂₃N₈O Requires: 391.1995). Purity by HPLC: 98.5% (t_R 24.03 min).

4.3.2.12. 6-(2-Aminoimidazolino)-6'-[2-(propyl)guanidino]dipiridiny-3-methane dihydrochloride (**8c**). Following **Method A**, to a solution of 4 M HCl/1,4-dioxane (18.0 eq., 378 μ L, 1.52 mmol) was added compound **19i** (1.0 eq., 55 mg, 0.084 mmol) affording the title compound as a yellow solid (30 mg, 85%). Mp: 148–151 °C decomposed. δ_{H} (400 MHz, D₂O): 0.81 (t, 3H, $J = 7.4$, CH₃), 1.50 (m, 2H, CH₂), 3.11 (t, 2H, $J = 7.4$, CH₂), 3.62 (s, 2H, CH₂), 3.66 (s, 4H, CH₂), 6.75 (d, 2H, $J = 8.4$, Ar), 7.45 (m, 2H, Ar), 7.94 (d, 1H, $^4J = 2.2$, Ar), 8.00 (d, 1H, $^4J = 2.2$, Ar). δ_{C} (100 MHz, D₂O): 10.3 (CH₃), 21.1 (CH₂), 30.1 (CH₂), 33.7 (CH₂), 42.7 (CH₂), 111.0 (CH Ar), 112.6 (CH Ar), 130.2 (q Ar), 132.0 (qC Ar), 139.7 (CH Ar), 139.8 (CH Ar), 145.7 (CH Ar), 148.8 (CH Ar), 148.8 (qC Ar), 151.6 (qC Ar), 156.0 (qC CN), 156.5 (qC CN). ν_{max} (ATR)/cm⁻¹: 3280 (NH), 2918, 1629, 1601, 1483, 1348, 1281, 1243, 1044, 1027, 1025, 926, 829, 741. HRMS: (m/z ESI⁺): Found: 353.2206 (M⁺ + H, C₁₈H₂₅N₈ Requires: 353.2202). Purity by HPLC: 98.5% (t_R 23.93 min).

4.3.2.13. 2-(2-Aminoimidazolino)-5-(4-guanidino)benzylpyridine dihydrochloride (**8d**). Following **Method A**, to a solution of 4 M HCl/1,4-dioxane (24.0 eq., 660 μ L, 2.64 mmol) was added compound **19j** (1.0 eq., 80 mg, 0.11 mmol) affording the title compound as a white solid (41 mg, 98%). Mp: 167–170 °C decomposed. δ_{H} (400 MHz, D₂O): 3.67 (s, 4H, CH₂), 3.84 (s, 2H, CH₂), 6.79 (d, 1H, $J = 8.4$, Ar), 7.10 (d, 2H, $J = 8.3$, Ar), 7.19 (d, 2H, $J = 8.3$, Ar), 7.52 (dd, 1H, $^3J = 8.4$, $^4J = 2.2$, Ar), 8.07 (d, 1H, $^4J = 2.2$, Ar). δ_{C} (100 MHz, D₂O): 36.4 (CH₂), 42.2 (CH₂), 112.7 (CH Ar), 126.1 (CH Ar), 130.1 (CH Ar), 132.3 (qC Ar), 132.8 (qC Ar), 139.8 (CH Ar), 140.4 (qC Ar), 146.6 (CH Ar), 148.7 (qC Ar), 155.7 (qC CN), 156.2 (qC CN). ν_{max} (ATR)/cm⁻¹: 3136 (NH), 2923, 2853, 1575, 1629, 1603, 1485, 1391, 1242, 1144, 1079, 1023, 926. HRMS: (m/z ESI⁺): Found: 310.1781 (M⁺ + H, C₁₆H₂₀N₇ Requires: 310.1780). Purity by HPLC: 96.1% (t_R 21.05 min).

4.3.2.14. 2-[2-Aminoimidazolino]-5-[4-[3-(furan-2-ylmethyl)guanidino]benzyl]pyridine dihydrochloride (**8e**). Following **Method A**, to a solution of 4 M HCl/1,4-dioxane (18.0 eq., 320 μ L, 1.26 mmol) was added compound **19k** (1.0 eq., 44 mg, 0.07 mmol) affording the title compound as a yellow solid (26 mg, 80%). Mp: 122–130 °C decomposed. δ_{H} (400 MHz, D₂O): 3.64 (s, 4H, CH₂), 3.79 (s, 2H, CH₂), 4.30 (s, 2H, CH₂), 6.24 (d, 1H, $J = 2.8$, Ar), 6.28 (m, 1H, Ar), 6.77 (d, 1H, $J = 8.4$, Ar), 7.06 (d, 2H, $J = 9.0$, Ar), 7.17 (d, 2H, $J = 9.0$, Ar), 7.34 (br s, 1H, Ar), 7.50 (dd, 1H, $^3J = 8.4$, $^4J = 2.3$, Ar), 8.05 (d, 1H, $^4J = 2.3$, Ar). δ_{C} (100 MHz, D₂O): 36.7 (CH₂), 42.6 (CH₂), 47.6 (CH₂), 108.1 (CH Ar), 110.5 (CH Ar), 112.6 (CH Ar), 126.1 (CH Ar), 130.1 (CH Ar), 132.2 (qC Ar), 132.8 (qC Ar), 139.8 (CH Ar), 140.3 (qC Ar), 143.1 (CH Ar), 146.5 (CH Ar), 148.1 (qC Ar), 149.0 (qC Ar), 155.0 (qC CN), 156.3 (qC CN). ν_{max} (ATR)/cm⁻¹: 3199 (NH), 2923, 29854, 1636, 1599, 1511, 1242, 1147, 1076, 1016, 925, 742, 678. HRMS: (m/z ESI⁺): Found: 390.2038 (M⁺ + H, C₂₁H₂₄N₇O Requires: 390.2042). Purity by HPLC: 96.4% (t_R 23.95 min).

4.3.2.15. 2-(2-Aminoimidazolino)-5-[4-(2-propylguanidino)benzyl]pyridine dihydrochloride (**8f**). Following **Method A**, to a solution of 4 M HCl/1,4-dioxane (18.0 eq., 360 μ L, 1.44 mmol) was added compound **19l** (1.0 eq., 53 mg, 0.08 mmol) affording the title compound as a light yellow solid (30 mg, 87%). Mp: 175–179 °C decomposed. δ_{H} (400 MHz, D₂O): 0.78 (t, 3H, $J = 7.4$, CH₃), 1.47 (m, 2H, CH₂), 3.08 (m, 2H, CH₂), 3.67 (br s, 4H, CH₂), 3.87 (s, 2H, CH₂), 6.80 (d, 1H, $J = 8.4$, Ar), 7.08 (d, 2H, $J = 8.4$, Ar), 7.18 (d, 2H, $J = 8.4$, Ar), 7.53 (dd, 1H, $^3J = 8.4$, $^4J = 2.2$, Ar), 8.03 (d, 1H, $^4J = 2.2$, Ar). δ_{C} (100 MHz, D₂O): 9.9 (CH₃), 21.2 (CH₂), 36.8 (CH₂), 42.0 (CH₂), 43.0 (CH₂), 112.0 (CH Ar), 126.2 (qC Ar), 130.1 (CH Ar), 132.5 (qC Ar), 133.1 (qC Ar), 139.1 (CH Ar), 146.6 (CH Ar), 148.7 (qC Ar), 155.7 (qC CN). ν_{max} (ATR)/cm⁻¹: 3324 (NH), 2963, 2833, 1655, 1572, 1395, 1202, 1164, 1097, 1020, 774. HRMS: (m/z ESI⁺): Found: 352.2254 (M⁺ + H, C₁₉H₂₆N₇ Requires: 352.2250). Purity by HPLC: 97.0% (t_R 22.64 min).

4.3.2.16. 2-Guanidino-5-[(2-aminoimidazolino)benzyl]pyridine dihydrochloride (**8g**). Following **Method A**, to a solution of 4 M HCl/1,4-dioxane (24.0 eq., 480 μ L, 1.92 mmol) was added compound **23a** (1.0 eq., 53 mg, 0.08 mmol) affording the title compound as an off-white solid (25 mg, 82%). Mp: 155–159 °C decomposed. δ_{H} (400 MHz, D₂O): 3.58 (s, 4H, CH₂), 3.78 (s, 2H, CH₂), 6.78 (d, 1H, $J = 8.4$, Ar), 7.07 (d, 2H, $J = 8.3$, Ar), 7.18 (d, 2H, $J = 8.3$, Ar), 7.50 (dd, 1H, $^3J = 8.4$, $^4J = 2.2$, Ar), 8.03 (d, 1H, $^4J = 2.2$, Ar). δ_{C} (100 MHz, D₂O): 36.8 (CH₂), 42.6 (CH₂), 113.5 (CH Ar), 124.5 (CH Ar), 130.0 (CH Ar), 132.9 (qC Ar), 133.4 (qC Ar), 139.5 (qC Ar), 140.0 (CH Ar), 146.0 (CH Ar), 149.2 (qC Ar), 158.0 (qC CN). ν_{max} (ATR)/cm⁻¹: 3338 (NH), 2934, 1652, 1606, 1492, 1391, 1240, 1068, 1025, 845, 757. HRMS (m/z ESI⁺): Found: 310.1783 (M⁺ + H, C₁₆H₂₀N₇ Requires: 310.1775). Purity by HPLC: 98.8% (t_R 21.47 min).

4.3.2.17. 2-[2-(Furan-2-ylmethyl)guanidino]-5-[4-(2-aminoimidazolino)benzyl]pyridine dihydrochloride (**8h**). Following **Method A**, to a solution of 4 M HCl/1,4-dioxane (18.0 eq., 315 μ L, 1.26 mmol) was added compound **23b** (1.0 eq., 47 mg, 0.07 mmol) affording the title compound as an off-white solid (29 mg, 90%). Mp: 134–137 °C, decomposed. δ_{H} (400 MHz, D₂O): 3.75 (s, 4H, CH₂), 3.91 (s, 2H, CH₂), 4.55 (s, 2H, CH₂), 6.47 (br s, 2H, Ar), 6.90 (d, 1H, $J = 8.5$, Ar), 7.20 (d, 2H, $J = 8.1$, Ar), 7.29 (d, 2H, $J = 8.1$, Ar), 7.53 (br s, 1H, Ar), 7.61 (dd, 1H, $^3J = 8.4$, $^4J = 1.6$, Ar), 8.07 (d, 1H, $^4J = 1.6$, Ar). δ_{C} (100 MHz, D₂O): 36.8 (CH₂), 37.8 (CH₂), 42.6 (CH₂), 108.4 (CH Ar), 110.6 (CH Ar), 113.2 (CH Ar), 124.3 (CH Ar), 129.9 (CH Ar), 132.7 (qC Ar), 133.3 (qC Ar), 139.6 (qC Ar), 139.9 (CH Ar), 143.3 (CH Ar), 145.7 (CH Ar), 148.7 (qC Ar), 149.6 (qC Ar), 153.9 (qC CN), 158.4 (qC CN). ν_{max} (ATR)/cm⁻¹: 3337 (NH), 2945, 2834, 1655, 1449, 1019, 1113, 1045, 956, 729. HRMS (m/z ESI⁺): Found: 390.2051 (M⁺ + H, C₂₁H₂₄N₇O Requires: 390.2037). Purity by HPLC: 98.6% (t_R 24.91 min).

4.3.2.18. 2-[2-(Propyl)guanidino]-5-[4-(2-aminoimidazolino)benzyl]pyridine dihydrochloride (**8i**). Following **Method A**, to a solution of 4 M HCl/1,4-dioxane (18.0 eq., 315 μ L, 1.26 mmol) was added compound **23c** (1.0 eq., 47 mg, 0.07 mmol) affording the title compound as a yellow solid (27 mg, 98%). Mp: 164–168 °C, decomposed. δ_{H} (400 MHz, D₂O): 0.78 (t, 3H, $J = 7.4$, CH₃), 1.47 (m, 2H, CH₂), 3.08 (m, 2H, CH₂), 3.67 (m, 4H, CH₂), 3.87 (s, 2H, CH₂), 6.80 (d, 1H, $J = 8.4$, Ar), 7.08 (d, 2H, $J = 8.4$, Ar), 7.18 (d, 2H, $J = 8.4$, Ar), 7.53 (dd, 1H, $^3J = 8.4$, $^4J = 2.2$, Ar), 8.03 (d, 1H, $^4J = 2.2$, Ar). δ_{C} (100 MHz, D₂O): 9.9 (CH₃), 21.3 (CH₂), 36.8 (CH₂), 42.6 (CH₂), 42.7 (CH₂), 112.9 (CH Ar), 124.3 (CH Ar), 127.5 (qC Ar), 129.8 (CH Ar), 133.4 (qC Ar), 139.5 (CH Ar), 139.7 (qC Ar), 145.5 (CH Ar), 149.5 (qC Ar), 153.3 (qC CN), 158.6 (qC CN). ν_{max} (ATR)/cm⁻¹: 3350 (NH), 2955, 2921, 1650, 1606, 1509, 1492, 1391, 1278, 1034, 837, 736. HRMS (m/z ESI⁺): Found: 352.2243 (M⁺ + H, C₁₉H₂₆N₇ Requires: 352.2244). Purity by HPLC: 98.8% (t_R 23.23 min).

Declaration of competing interest

The authors declare that they have no known competing financial interests or personal relationships that could have appeared to influence the work reported in this paper.

Acknowledgments

Thanks are given to the School of Chemistry at Trinity College Dublin (M.McM.) and to the Irish Research Council (A.K. -GOIPG/2014/457- and H.B.M. -GOIPG/2017/834-) for postgraduate support. This study was also supported by the Ministerio de Economía y Competitividad of Spain (SAF2013-48586-R) and the Basque Government (IT1211-19). The authors would like to thank the staff members of the Basque Institute of Legal Medicine for their cooperation in the study.

Appendix A. Supplementary data

Supporting Information is available for the calculated total energies, synthetic procedures and spectroscopic data for all intermediates and NMR spectra and HPLC chromatograms of all the final hydrochloride salts.

Supplementary data to this article can be found online at <https://doi.org/10.1016/j.ejmech.2020.112947>.

References

- [1] E.J. Nestler, The biological basis of depression: insights from animal models, in: J.J. Strain, M. Blumenfeld (Eds.), *Depression as a Systemic Illness*, Oxford University Press, New York, 2018, pp. 1–13.
- [2] F. Cathomas, J.W. Murrough, E.J. Nestler, M.-H. Han, S.J. Russo, Neurobiology of resilience: interface between mind and body, *Biol. Psychiatr.* 86 (2019) 410–420.
- [3] C.H. Stanton, A.J. Holmes, S.W.C. Chang, J. Joermann, From stress to anhedonia: molecular processes through functional circuits, *Trends Neurosci.* 42 (2019) 23–42.
- [4] G. Di Giovanni, D. Svob Strac, M. Sole, M. Unzeta, K.F. Tipton, D. Mück-Šeler, I. Bolea, L. Della Corte, M. Nikolac Perkovic, N. Pivac, I.J. Smolders, A. Stasiak, W.A. Fogel, P. De Deurwaerdere, Monoaminergic and histaminergic strategies and treatments in brain diseases, *Front. Neurosci.* 10 (2016) 541.
- [5] S.R. Wainwright, L.A. Galea, The neural plasticity theory of depression: assessing the roles of adult neurogenesis and PSA-NCAM within the hippocampus, *Neural Plast.* 2013 (2013), 805497.
- [6] S.A. Flavin, D.G. Winder, Noradrenergic control of the bed nucleus of the stria terminalis in stress and reward, *Neuropharmacology* 70 (2013) 324–330.
- [7] C. Cottingham, Q. Wang, $\alpha 2$ Adrenergic receptor dysregulation in depressive disorders: implications for the neurobiology of depression and antidepressant therapy, *Neurosci. Biobehav. Rev.* 36 (2012) 2214–2225.
- [8] V. Maletic, A. Eramo, K. Gwin, S.J. Offord, R.A. Duffy, The role of norepinephrine and its α -adrenergic receptors in the pathophysiology and treatment of major depressive disorder and Schizophrenia: a systematic review, *Front. Psychiatr.* 8 (2017) 42.
- [9] J. García-Sevilla, P. Ventayol, V. Pérez, G. Rubovszky, D. Puigdemont, M. Ferrer-Alcón, A. Andreoli, J. Guimón, E. Alvarez, Regulation of platelet $\alpha 2A$ -adrenoceptors, Gi proteins and receptor kinases in major depression: effects of Mirtazapine treatment, *Neuropsychopharmacol* 29 (2004) 580–588.
- [10] F. Rodríguez, I. Rozas, J.E. Ortega, J.J. Meana, L.F. Callado, Guanidine and 2-aminoimidazole aromatic derivatives as $\alpha 2$ -adrenoceptor antagonists, 1: towards new antidepressants with heteroatomic linkers, *J. Med. Chem.* 50 (2007) 4516–4527.
- [11] F. Rodríguez, I. Rozas, J.E. Ortega, A.M. Erdozain, J.J. Meana, L.F. Callado, Guanidine and 2-aminoimidazole aromatic derivatives as $\alpha 2$ -adrenoceptor antagonists, 2: exploring alkyl linkers for new antidepressants, *J. Med. Chem.* 51 (2008) 3304–3312.
- [12] F. Rodríguez, I. Rozas, J.E. Ortega, A.M. Erdozain, J.J. Meana, L.F. Callado, Guanidine and 2-aminoimidazole aromatic derivatives as $\alpha 2$ -adrenoceptor ligands: searching for Structure-Activity relationship, *J. Med. Chem.* 52 (2009) 601–609.
- [13] D.H. O'Donovan, C. Muguruza, L.F. Callado, I. Rozas, Guanidine-based $\alpha 2$ -adrenoceptor ligands: towards selective antagonist activity, *Eur. J. Med. Chem.* 82 (2014) 242–254.
- [14] B. Kelly, M. McMullan, C. Muguruza, J.E. Ortega, J.J. Meana, L.F. Callado, I. Rozas, $\alpha 2$ -Adrenoceptor antagonists: synthesis, pharmacological evaluation and molecular modelling investigation of pyridinyl guanidine/2-aminoimidazole and their derivatives, *J. Med. Chem.* 58 (2015) 963–977.
- [15] M. McMullan, A. García-Bea, P. Miranda-Azpiazu, L.F. Callado, I. Rozas, Substituted conformationally restricted guanidine derivatives: probing the $\alpha 2$ -adrenoceptors' binding pocket, *Eur. J. Med. Chem.* 123 (2016) 48–57.
- [16] M.P. Groziak, L.B. Townsend, A new and efficient synthesis of guanosine, *J. Org. Chem.* 51 (1986) 1277–1282.
- [17] L.F. Callado, J.J. Meana, Low-affinity conditions for agonists increase the binding of the antagonist [3H]RX821002 to the $\alpha 2B/C$ -adrenoceptor subtypes in human brain and rat kidney, *Eur. J. Pharmacol.* 332 (1997) 109–112.
- [18] P. Marini, M.-G. Cascio, A. King, R.G. Pertwee, R.A. Ross, Characterization of cannabinoid receptor ligands in tissues natively expressing cannabinoid CB2 receptors, *British J. Pharmacol.* 169 (2013) 887–899.
- [19] Schrödinger Release 2016-1: Prime, Schrödinger, LLC, New York, NY, 2016.
- [20] D.P. Staus, R.T. Strachan, A. Manglik, B. Pani, A.W. Kahsai, T.H. Kim, L.M. Wingler, S. Ahn, A. Chatterjee, A. Masoudi, A.C. Kruse, E. Pardon, J. Steyaert, W.I. Weis, R.S. Prosser, B.K. Kobilka, T. Costa, R.J. Lefkowitz, Nature 535 (2016) 448–452.
- [21] R.A. Friesner, R.B. Murphy, M.P. Repasky, L.L. Frye, J.R. Greenwood, T.A. Halgren, P.C. Sanschagrin, D.T. Mainz, Extra precision Glide: docking and scoring incorporating a model of hydrophobic enclosure for protein-ligand complexes, *J. Med. Chem.* 49 (2006) 6177–6196.
- [22] J.A. Ballesteros, H. Weinstein, Integrated methods for the construction of three-dimensional models and computational probing of structure-function relations in G protein-coupled receptors, *Methods Neurosci.* 25 (1995) 366–428.
- [23] G. Pándy-Szekeres, C. Munk, T.M. Tsonkov, S. Mordalski, K. Harpsøe, A.S. Hauser, A.J. Bojarski, D.E. Gloriam, GPCRdb in 2018: adding GPCR structure models and ligands, *Nucleic Acids Res.* 46 (2017) D440–D446.
- [24] M. Masureel, Y. Zou, L.P. Picard, E. van der Westhuizen, J.P. Mahoney, J.P.G.L.M. Rodrigues, T.J. Mildorf, R.O. Dror, D.E. Shaw, M. Bouvier, E. Pardon, J. Steyaert, R.K. Sunahara, W.I. Weis, C. Zhang, B.K. Kobilka, Structural insights into binding specificity, efficacy and bias of a $\beta 2AR$ partial agonist, *Nat. Chem. Biol.* 14 (2018) 1059–1066.
- [25] L. Qu, Q.T. Zhou, Y. Xu, Y. Guo, X.Y. Chen, D. Yao, G.W. Han, Z.-J. Liu, R.C. Stevens, G.S. Zhong, D. Wu, S.W. Zhao, Structural basis of the diversity of adrenergic receptors, *Cell Rep.* 29 (2019), 2929–2935 and 2936–2943.
- [26] Qu, L.; Zhou, Q. T.; Wu, D.; Zhao, S.W. Crystal structures of the $\alpha 2A$ adrenergic receptor in complex with an antagonist RSC. Released in PDB the 4th of December 2019. To Be Published. DOI: 10.2210/pdb6KUX/pdb.
- [27] Chen, X. Y.; Wu, D.; Wu, L. J.; Han, G. W.; Guo, Y.; Zhong, G. S. Crystal structure of human $\alpha 2C$ adrenergic G protein-coupled receptor. Released in PDB the 4th of December 2019. To be published. DOI: 10.2210/pdb6KUW/pdb.
- [28] D. Yuan, Z. Liu, J. Kaindl, S. Maeda, J. Zhao, X. Sun, J. Xu, P. Gmeiner, H.W. Wang, B.K. Kobilka, Activation of the $\alpha 2B$ -adrenoceptor by the sedative sympatholytic dexmedetomidine, *Nat. Chem. Biol.* 16 (2020) 507–512.
- [29] C. Muguruza, F. Rodríguez, I. Rozas, J.J. Meana, L. Uriguen, L.F. Callado, Anti-depressant-like properties of three new $\alpha 2$ -adrenoceptor antagonists, *Neuropharmacology* 65 (2013) 13–19.
- [30] A. Šali, T.L. Blundell, Comparative protein modelling by satisfaction of spatial restraints, *J. Mol. Biol.* 234 (1993) 779–815.
- [31] M.A. Lomize, I.D. Pogozheva, H. Joo, H.I. Mosberg, A.L. Lomize, OPM database and PPM web server: resources for positioning of proteins in membranes, *Nucleic Acids Res.* 40 (2012) D370–D376.
- [32] J. Gumbart, L.G. Trabuco, E. Schreiner, E. Villa, K. Schulten, Regulation of the protein-conducting channel by a bound ribosome, *Structure* 17 (2009) 1453–1464.
- [33] J. Huang, A.D. MacKerell Jr., CHARMM36 all-atom additive protein force field: validation based on comparison to NMR data, *J. Comput. Chem.* 34 (2013) 2135–2145.
- [34] K. Vanommeslaeghe, E. Hatcher, C. Acharya, S. Kundu, S. Zhong, J. Shim, E. Darian, O. Guvench, P. Lopes, I. Vorobyov, A.D. MacKerell Jr., CHARMM general force field: a force field for drug-like molecules compatible with the CHARMM all-atom additive biological force fields, *J. Comput. Chem.* 31 (2010) 671–690.
- [35] C.W. Hopkins, S. Le Grand, R.C. Walker, A.E. Roitberg, Long-time-step molecular dynamics through hydrogen mass repartitioning, *J. Chem. Theor. Comput.* 11 (2015) 1864–1874.
- [36] D.A. Case, J.T. Berryman, R.M. Betz, D.S. Cerutti, T.E. Cheatham III, T.A. Darden, R.E. Duke, T.J. Giese, H. Gohlke, A.W. Goetz, N. Homeyer, S. Izadi, P. Janowski, J. Kaus, A. Kovalenko, T.S. Lee, S. LeGrand, P. Li, T. Luchko, R. Luo, B. Madej, K.M. Merz, G. Monard, P. Needham, H. Nguyen, H.T. Nguyen, I. Omelyan, A. Onufriev, D.R. Roe, A. Roitberg, R. Salomon-Ferrer, C.L. Simmerling, W. Smith, J. Swails, R.C. Walker, J. Wang, R.M. Wolf, X. Wu, D.M. York, P.A. Kollman, AMBER 2015, University of California, San Francisco, 2015.
- [37] W. Humphrey, A. Dalke, K. Schulten, VMD - visual molecular dynamics, *J. Mol. Graph.* 14 (1996) 33–38.
- [38] D.R. Roe, T.E. Cheatham III, PTRAJ and CPPTRAJ: software for processing and analysis of molecular dynamics trajectory data, *J. Chem. Theor. Comput.* 9 (2013) 3084–3095.
- [39] The PyMOL Molecular Graphics System, Version 2.0 Schrödinger, LLC.
- [40] A.I. Vogel, A.R. Tatchell, B.S. Furnis, A.J. Hannaford, Vogel's Textbook of Practical Organic Chemistry, fifth ed., 1996.